

Simultaneous Detection of Ozone and Nitrogen Dioxide by Oxygen Anion Chemical Ionization Mass Spectrometry: A Fast Time Response Sensor Suitable for Eddy Covariance Measurements

Gordon A. Novak, Michael P. Vermeuel, Timothy H. Bertram

5 Department of Chemistry, University of Wisconsin – Madison, Madison, WI, USA

Correspondence to: Timothy H. Bertram (timothy.bertram@wisc.edu)

Abstract. We report on the development, characterization, and field deployment of a fast time response sensor for measuring ozone (O_3) and nitrogen dioxide (NO_2) concentrations utilizing chemical ionization time-of-flight mass spectrometry (CI-ToFMS) with oxygen anion (O_2^-) reagent ion chemistry. We demonstrate that the oxygen anion chemical ionization mass spectrometer (Ox-CIMS) is highly sensitive to both O_3 (180 ~~ions-counts~~ s^{-1} pptv $^{-1}$) and NO_2 (97 ~~ions-counts~~ s^{-1} pptv $^{-1}$),
10 corresponding to detection limits (3σ , 1 s averages) of 13 and 9.9 pptv, respectively. In both cases, the detection threshold is limited by the magnitude and variability in the background determination. The short-term precision (1 s averages) is better than 0.3% at 10 ppbv O_3 and 4% at 10 pptv NO_2 . We demonstrate that the sensitivity of the O_3 measurement to fluctuations in ambient water vapor and carbon dioxide is negligible for typical conditions encountered in the troposphere. The application of
15 the Ox-CIMS to the measurement of O_3 vertical fluxes over the coastal ocean, via eddy covariance (EC), was tested during summer 2018 at Scripps Pier, La Jolla CA. The observed mean ozone deposition velocity ($v_d(O_3)$) was 0.0134 $cm\ s^{-1}$ with a campaign ensemble limit of detection (LOD) of 0.002742 $cm\ s^{-1}$ at the 95% confidence level, from each 27-minute sampling period LOD. The campaign mean and one standard deviation range of O_3 mixing ratios were $41.238.9 \pm 102.13$ ppbv. Several
20 fast ozone titration events from local NO emissions were sampled where unit conversion of O_3 to NO_2 was observed, highlighting instrument utility as a total odd oxygen ($O_x = O_3 + NO_2$) sensor. The demonstrated precision, sensitivity, and time resolution of this instrument highlight its potential for direct measurements of O_3 ocean–atmosphere and biosphere–atmosphere exchange from both stationary and mobile sampling platforms.

1 Introduction

The deposition of O_3 to the ocean surface is a significant component of the tropospheric ozone budget. Global chemical
25 transport model studies that explicitly treat O_3 deposition, indicate that approximately one-third of total ozone dry deposition is to water surfaces (Ganzeveld et al., 2009). However, the magnitude of total annual global ozone deposition to ocean surfaces is highly sensitive to the deposition velocity parameterization used, with model estimates ranging from 95 to 360 Tg yr $^{-1}$ (Ganzeveld et al., 2009; Luhar et al., 2017). Several common global chemical transport models including GEOS-Chem (Bey et al., 2001), MOZART-4 (Emmons et al., 2010), and CAM-chem (Lamarque et al., 2012) apply a globally uniform deposition
30 velocity (v_d) that ranges between 0.01–0.05 $cm\ s^{-1}$ depending on the model. In comparison to terrestrial measurements, where

O₃ dry deposition velocities are relatively fast (>0.1 cm s⁻¹, (Zhang et al., 2003), there is a paucity of direct observations of ozone deposition to the ocean surface necessary to constrain atmospheric models. Previous studies of O₃ deposition to water surfaces have been made from coastal towers (Gallagher et al., 2001), aircraft (Faloona et al., 2005; Kawa and Pearson, 1989; Lenschow et al., 1981), underway research vessels (Helmig et al., 2012), and in the laboratory (McKay et al., 1992), with observed $v_d(\text{O}_3)$ ranging between 0.01 and 0.15 cm s⁻¹. There is only one reported study of O₃ deposition to freshwater, which showed $v_d(\text{O}_3)$ of 0.01 cm s⁻¹ (Wesely et al., 1981). Measured deposition rates to snow and ice vary widely, with most observations of $v_d(\text{O}_3)$ from 0 to 0.2 cm s⁻¹, while models suggest $v_d(\text{O}_3)$ from 0 to 0.01 cm s⁻¹ (Helmig et al., 2007). Reactions of O₃ with iodide and dissolved organic compounds (DOC) in the ocean are known to play a controlling role in setting $v_d(\text{O}_3)$ and may explain some of the variability in observations (Chang et al., 2004; Ganzeveld et al., 2009). However, these quantities have not typically been measured during field studies of $v_d(\text{O}_3)$. To date there is no consensus on whether measured ocean O₃ deposition velocities show a wind speed dependence (Fairall et al., 2007). The most comprehensive dataset is from Helmig et al., (2012), which reported a deposition velocity range of 0.009 – 0.034 cm s⁻¹ from 1700 hours of observation over five research cruises. This dataset showed variability of $v_d(\text{O}_3)$ with wind speed (U_{10}) and sea–surface temperature (SST), highlighting the need for further field observations as constraints for model parameterizations.

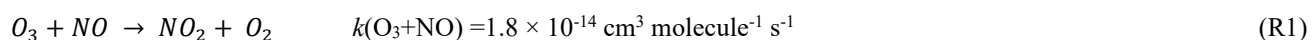
The small magnitude of O₃ ocean–atmosphere vertical fluxes presents a significant analytical challenge for existing ozone sensors used in eddy covariance (EC) analyses. Driven in part by stringent sensor requirements for EC techniques, significant uncertainties in the magnitude and variability of ozone deposition to water surfaces remain. In contrast, O₃ vertical fluxes to terrestrial surfaces are 10 to 100 times faster than to water surfaces, significantly loosening sensor precision requirements. Nonetheless, significant variability in $v_d(\text{O}_3)$ exists between surface types (e.g. soil vs. leaf) (Wesely and Hicks, 2000). Terrestrial deposition velocities also show strong diel and seasonal variability due to factors such as stomatal opening and within-canopy chemistry (Fares et al., 2010; Fowler et al., 2001; Kurpius and Goldstein, 2003). Highly accurate and precise measurements of O₃ are required to correctly model the response of $v_d(\text{O}_3)$ to each of these factors. While terrestrial and ocean exchange studies have substantial differences in experimental design, a sensor suitable for ocean–atmosphere ozone deposition measurements *via* EC is expected to be highly capable of biosphere–atmosphere measurements due to the significantly larger deposition rates and similar accuracy requirements.

Eddy covariance measurements typically require fast (1-10 Hz), high precision sensors in order to resolve covariance on the timescales of the fastest atmospheric turbulent eddies. Due to this constraint, standard O₃ monitoring instruments which utilize UV-absorption detection do not have suitable time response or precision for EC measurements and ozone flux measurements have primarily utilized fast response chemiluminescence sensors. Chemiluminescence detectors can use either gas-phase, dry, or wet, dry, or gas-phase reagents for detection with important differences between them (Muller et al., 2010). Gas-phase chemiluminescence sensors are typically based on the reaction of O₃ with nitric oxide (NO) to form an excited state NO₂* which then relaxes to the ground state, emitting a photon that can be detected. This method has well understood reaction kinetics and allows for high sensitivity detection on the order of 2.8 counts s⁻¹ pptv⁻¹ (Bariteau et al., 2010; Pearson, 1990). A practical disadvantage to this technique is the necessity of a compressed cylinder of NO which is highly toxic. Wet

65 chemiluminescence techniques are used less, as they exhibit generally lower sensitivity than dry chemiluminescence sensors and can be limited by issues in the liquid flow (Keronen et al., 2003).

Dry chemiluminescence sensors have the simplest operation and have seen the most regular use for EC studies (Güsten et al., 1992; Tuovinen et al., 2004). However, dry chemiluminescence sensor discs require conditioning with high ozone (up to 400 ppbv for several hours) before operation, are known to degrade over time, and have high variability in
70 sensitivity between sensor discs (Weinheimer, 2007). These factors have led to limitations in long term stability and to uncertainty in calibration factors for dry chemiluminescence sensors, resulting in uncertainty in the accuracy of the flux measurement (Muller et al., 2010). Muller et al.(2010), also reported a comparison of two identical co-located dry chemiluminescence sensors with half-hourly flux values differing by up to a factor of two and a mean hourly flux difference ranging from 0 to 23% between sensors. Recently Zahn et al., (2012) reported the development of a commercial dry
75 chemiluminescence ozone detector capable of fast (>10 Hz) measurements with high sensitivity ($\sim 9 \text{ counts s}^{-1} \text{ pptv}^{-1}$) suitable for EC or mobile platform sampling. However, they also report issues of short- and long-term drift and variability between sensor discs. These accuracy and drift concerns have driven an interest in the development of a new, stable and fast ozone sensor suitable for EC measurements from both stationary and mobile sampling platforms.

In addition to the inherently small magnitude of $v_d(\text{O}_3)$, the fast chemical titration of O_3 by NO (R1) often complicates
80 the interpretation of $v_d(\text{O}_3)$ measurements. Surface emissions of NO result in a high bias in the measured deposition velocity when the titration reaction (R1) is fast relative to the transport time to the height of the sensor.



Surface NO emissions from both biogenic and anthropogenic sources are widespread, with ocean emissions on the order of $1 \times 10^8 \text{ molecules cm}^{-2} \text{ s}^{-1}$ (Zafiriou and McFarland, 1981) and soil emissions ranging from 5×10^9 to $2 \times 10^{11} \text{ molecules cm}^{-2}$
85 s^{-1} (Yienger and Levy, 2004). These emissions correspond to a positive bias in the observed $v_d(\text{O}_3)$ dry deposition rate on the order of 5% in the marine atmosphere (discussed in section 3.7.1) and up to 50% in a forested site (Dorsey et al., 2004). Simultaneous flux detection of O_3 with one or both of NO or NO_2 is commonly used to address this flux divergence problem (Finco et al., 2018; Stella et al., 2013). However, these studies typically require separate sensors for O_3 and NO_x which can introduce additional sources of uncertainty. Related challenges of fast O_3 titration exists for quantification of O_3 from mobile
90 platforms where there is dynamic sampling of different airmasses with potentially differing O_3 –NO– NO_2 steady-state conditions.

In what follows, we describe the characterization and first field observations of a novel oxygen anion chemical ionization time-of-flight mass spectrometer (Ox-CIMS) sensor for O_3 and NO_2 . Over the past two decades, chemical ionization mass spectrometry (CIMS) techniques have emerged as sensitive, selective, and accurate detection methods for a diverse suite
95 of reactive trace gases (Huey, 2007). Successful application of CIMS for EC flux measurements have been demonstrated from many sampling platforms including ground sites (Kim et al., 2014; Nguyen et al., 2015), aircraft (Wolfe et al., 2015), and underway research vessels (Blomquist et al., 2010; Kim et al., 2017; Yang et al., 2013) employing a variety of reagent ion

chemistry systems. Here we demonstrate the suitability of the Ox-CIMS for EC flux measurements and provide detailed laboratory characterization of the instrument.

100 2 Laboratory Characterization

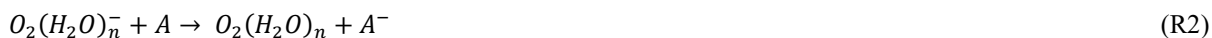
2.1 Chemical-ionization time-of-flight mass spectrometer

A complete description of the CI-ToFMS instrument (Aerodyne Research Inc., TOFWERK AG) can be found in Bertram et al. (2011). In what follows we highlight significant differences in the operation of the instrument from what is discussed in Bertram et al., (2011). Oxygen anions are generated by passing an 11:1 volumetric blend of Ultrahigh Purity (UHP) N₂ and O₂ gas (both Airgas 5.0 grade) through a polonium-210 α -particle source (NRD, P-2021 Ionizer). This N₂:O₂ volume ratio was found empirically to maximize total reagent ion signal in our instrument while minimizing background signal at the O₃ detection product (CO₃⁻, -60 m/Q). Further discussion of the reagent ion chemistry and precursor concentration can be found in sections 2.2 and 2.8. The reagent ion stream then mixes with ambient air in an ion-molecule reaction (IMR) chamber held at 95 mbar where product ions were generated. Further discussion of the dependence of instrument sensitivity on IMR pressure can be found in section 2.6. At this pressure, the residence time in the IMR is estimated to be on the order of 100 ms. Product ions then pass into three differentially pumped chambers before reaching the ToF mass analyzer. Ions first move from the IMR to a collisional dissociation chamber (CDC) held at 2 mbar which houses a short-segmented RF-only quadrupole ion guide. Field strengths in the IMR and CDC were tuned to be as soft as possible to preserve the transmission of weakly bound clusters while still maintaining acceptable total ion signals (ion optic potentials are listed in Table S1). Ions then sequentially pass into a second RF-only quadrupole chamber held at 1.4×10^{-2} mbar and a final chamber containing focusing optics which prepare the ion beam for entry into the compact ToF mass analyzer (CToF, TOFWERK AG and Aerodyne Research Inc.). The mass resolving power ($M/\Delta M$) of the instrument as configured for these experiments was greater than 900 at -60 m/Q. All ion count rates reported here are for unit mass resolution integrated peak areas. In this work extraction frequencies of 75 kHz were used, resulting in mass spectra from 27-327 -m/Q. All mass spectra were saved at 10 Hz for analysis.

120 2.2 Oxygen Anion Chemistry

Oxygen anion (O₂⁻) reagent ion chemistry has been investigated previously for its use in the detection of nitric acid and more recently hydrogen peroxide (Huey, 1996; O'Sullivan et al., 2018; Vermeuel et al., 2019). Oxygen anion chemistry has also been used for chemical analysis of aerosol particles in a thermal desorption instrument, primarily for detection of particle sulfate and nitrate (Voisin et al., 2003). Oxygen anion chemistry has also been used for the detection of SO₂ *via* a multi-step ionization process where CO₃⁻ reagent ions are first generated by the reaction of O₂⁻ with added excess O₃ in the presence of CO₂. The CO₃⁻ reagent ion product then ligand switches with SO₂ to form SO₃⁻ which then quickly reacts with ambient O₂ to

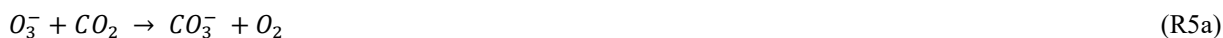
form the primary detected SO_5^- product (Porter et al., 2018; Thornton et al., 2002a). Ionization of analytes by oxygen anion reagent ion chemistry proceeds through both charge transfer (R2) and adduct formation (R3).



It is expected that charge transfer from oxygen will occur to any analyte with an electron affinity (E.A.) greater than O_2 (0.45 eV, (Ervin et al., 2003)) resulting in a relatively non-specific reagent ion chemistry (see (Rienstra-Kiracofe et al., (2002) for a compilation of molecular E.A. values), which is sensitive to a wide class of molecules. Adduct formation is observed when the binding enthalpy of the adduct is larger than that of the oxygen-water adduct and the adduct is stable enough to be preserved through the ion optics. This adduct formation framework is analogous to what has been shown for iodide reagent ion chemistry (Lee et al., 2014).

The O_2^- reagent ions present in the IMR are expected to have a series of attached water molecules at ambient humidity and the IMR pressure (95 mbar) and electric field strengths used in this study (Bork et al., 2011). The reagent ion is therefore reported as $\text{O}_2(\text{H}_2\text{O})_n^-$ for the remainder of this work. In the recorded mass spectra from our instrument, all reagent ion signal is observed as $n = 0-1$ (i.e., O_2^- and $\text{O}_2(\text{H}_2\text{O})^-$) as seen in Fig. 1. Oxygen anion-water clusters larger than $n = 1$ are likely present in the IMR but H_2O evaporates off of the cluster in the CDC before detection due to the lower binding enthalpy of each additional water in $\text{O}_2(\text{H}_2\text{O})_n^-$ (Bork et al., 2011) and the high field strength at the exit of the CDC (Brophy and Farmer, 2016). Variability in the number of attached water molecules (n) as a function of humidity introduces the possibility of a water dependence on the ion chemistry, which is discussed further in Section 2.5.

145 The detection of ozone (O_3) by oxygen anion reagent ion chemistry proceeds *via* a two-step reaction leading to the formation of a carbonate anion (CO_3^-), which is the final detected product. First, the oxygen anion ($\text{O}_2(\text{H}_2\text{O})_n^-$) either transfers an electron to ozone forming O_3^- (R4a) or forms a stable cluster with ozone (R4b). The ozone anion (either bare or as a cluster with $\text{O}_2(\text{H}_2\text{O})_n^-$) then reacts with a neutral CO_2 molecule to form CO_3^- (R5a–5b) which is the primary, detected product in the mass spectrometer. The electron affinity of O_3 is 2.1 eV (Arnold et al., 1994).



It is not clear whether it is the bare ozone anion (R4a & R5a) or the cluster (R4b & R5b) that goes on to react with CO_2 to form the carbonate anion. The $\text{O}_2(\text{O}_3)(\text{H}_2\text{O})_n^-$ product has not been observed in the mass spectrometer, but it may exist in the IMR and dissociate as it transfers into the CDC prior to detection. A small amount of ozone is detected directly as O_3^- but the magnitude of this signal is less than 1% of the signal of CO_3^- during ambient sampling. The proposed mechanism of CO_3^- formation is supported by a study using isotopically labelled oxygen to form labelled ozone anions ($^{18}\text{O}_3^-$) in a corona

discharge source which then reacted with CO₂ to form the detected product C¹⁸O₂⁻ (Ewing and Waltman, 2010). This product
160 supports that a single oxygen is transferred from the ozone anion to carbon dioxide (as in R5a).

The detection of NO₂ proceeds directly through a charge transfer reaction with O₂(H₂O)_n⁻ to form the detected NO₂⁻
product (R6). This is expected based upon the high E.A. of NO₂ (2.27 eV, (Ervin et al., 1988)) compared to O₂ (E.A 0.45 eV).



Oxygen anions are expected to be a highly general reagent ion chemistry, showing sensitivity to an array of analytes.
165 While the focus of this work is on detection of O₃ and NO₂, detection of hydrogen peroxide, nitric acid, formic acid, sulfur
dioxide and other species with the Ox-CIMS has demonstrated good performance (Vermeuel et al., 2019). An example ambient
mass spectrum recorded at 1 Hz sampling is shown in Fig. 1, with several major peaks highlighted. Also apparent are an
abundance of peaks throughout the spectra with high signal intensity. During ambient observations, over one third of masses
from -m/Q 27-327 showed signal intensity greater than 1 x 10⁴ counts per second (cps). A larger survey and classification of
170 oxygen anion reagent ion chemistry to utilize this versatility is underway.

2.3 Laboratory calibration

Laboratory calibrations of the Ox-CIMS were performed to determine instrument sensitivity to O₃ and NO₂. Ozone was
generated by passing UHP Zero Air (ZA, Airgas 5.0 grade) through a mercury lamp UV source (Jelight Co, Irvine CA).
Outflow from the lamp source was diluted in UHP ZA and split between the Ox-CIMS and a factory calibrated 2B POM ozone
175 monitor (2B Technologies) with an accuracy of ± 1.5 ppbv, which served as our reference standard. Ozone concentrations
were varied over the range 0–80 ppbv and instrument response was determined to generate a calibration curve. NO₂ was
delivered from a certified standard cylinder (Scott-Marrin 4.84 ± 0.1 ppmv). The primary NO₂ standard was diluted in UHP
ZA to span the range of 0–10 ppbv. Dilutions of calibration standards were made in UHP ZA which was humidified to the
desired amount by splitting a portion of the flow through a bubbler containing 18 MΩ water. CO₂ (Airgas Bone Dry grade)
180 was added to the dilution flow to maintain mixing ratios of 380 ppmv for all calibrations (See Section 2.6). A Vaisala HMP
110 sensor continuously measured relative humidity and temperature inline downstream of the Ox-CIMS and POM inlets. All
flows were controlled by mass flow controllers (MKS instruments, 1179C series) with an estimated total uncertainty of 10%.
Example calibration curves for O₃ and NO₂ are shown in Fig. 2. An overview of instrument sensitivity, limits of detection
(LOD), and precision to O₃ and NO₂ is given in Table 1.

185 2.4 Absolute sensitivity

The absolute sensitivity of the Ox-CIMS for detection of analytes is controlled by the kinetics and thermodynamics of the
reagent ion chemistry and the total ion generation and transmission efficiency of the instrument. Under the operational
configuration described in Section 2.1, typical reagent ion signal (O₂⁻ + O₂(H₂O)_n⁻) ranged from 0.8 to 2.2 × 10⁷ ~~countsiens~~
s⁻¹ (Fig. S1). The mean total reagent ion signal over 6 weeks of ambient sampling (Section 3.1) was 1.45 × 10⁷ ~~cpisens-s⁺~~
190 absolute instrument sensitivity at this reagent ion signal to O₃ and NO₂ is 180 and 97 ~~cpisens-s⁺~~ pptv⁻¹ respectively (at 8 g kg⁻¹

¹ SH). Total instrument count rate is a complex function of instrument design, instrument ion optics tuning, Po-210 source decay, micro channel plate (MCP) detector decay, and ToF extraction frequency; all of which are either tunable parameters or vary in time. Conversely, the reagent ion charge transfer or adduct formation chemistry for a given analyte sets a fundamental limit on sensitivity for a given instrument configuration. Sensitivity values can be normalized by scaling all signals to a fixed total reagent ion signal count rate of (1×10^6 cps ions-s⁻¹) to isolate the sensitivity component controlled by reagent ion chemistry, separate from changes in instrument performance due to decay in the ion source or other factors. total instrument count rate. The total reagent ion signal is taken as the sum of the O_2^- and $O_2(H_2O)^-$ signals. Sensitivity values through the remainder of the text are reported as either absolute sensitivities in counts per second (cps pptv⁻¹) or normalized sensitivities in normalized counts per second (ncps pptv⁻¹). Absolute sensitivity values control instrument limits of detection (LOD) and precision, while normalized sensitivities are used for comparison of calibration factors.

2.5 Dependence of instrument sensitivity on specific humidity

The dependence of instrument sensitivity on ambient water content was assessed for specific humidity (SH) ranging between 0–16 g kg⁻¹ (approximately 0–80% RH at 25 °C) by triplicate calibrations as shown in Fig. 3. Sensitivity to O₃ was seen to have had no significant dependence on specific humidity over the range 4–16 g kg⁻¹. Sensitivity to NO₂ has a specific humidity dependence over the range 4–16 g kg⁻¹, decreasing from 7.9 to 4.6 ncps pptv⁻¹. A 30% and 45% decline in sensitivity was observed from 0 to 4 g kg⁻¹ for O₃ and NO₂ respectively. This low humidity range is rarely sampled in the boundary layer over water surfaces but may be significant in some terrestrial or airborne deployments and would require careful calibration. The SH range from 8 to 16 g kg⁻¹ corresponds to approximately 40 to 80% RH at 25 °C which is typical of the humidity range over mid-latitude oceans (Liu et al., 1991). *Ab initio* calculations of $O_2^-(H_2O)_n$ and $O_3^-(H_2O)_n$ clusters performed by Bork et al. (2011) showed that charge transfer from the bare ($n=0$) O_2^- to O_3^- was exothermic at ca. -160 kJ/mol. At larger cluster sizes of $n = 4-12$, charge transfer becomes less favorable and converges to ca. -110 kJ/mol. An increase in n from 0 to 4 over the SH range 0–4 g kg⁻¹ is a potential explanation for the initial decline in sensitivity observed with SH before levelling off from 4–16 g kg⁻¹. It is not known if the enthalpy of charge transfer from $O_2^-(H_2O)_n$ to NO₂ follows a similar trend with n . Ion mobility studies to determine the $O_2^-(H_2O)_n$ cluster size with SH and IMR pressure would provide valuable insight on the observed dependence of sensitivity on water content.

2.6 Dependence on CO₂

The ionization pathway for detection of O₃ with $O_2^-(H_2O)_n$ reagent ion chemistry differs from typical chemical ionization schemes, in that it involves a two-step reaction of charge transfer to ozone forming O_3^- , which then reacts with CO₂ to form the detected CO_3^- product (R4-R5). Therefore, we assessed the impact of CO₂ mixing ratio in the sample flow on O₃ sensitivity as shown in Fig. 4. Calibration curves were generated by diluting ozone in dry UHP N₂ and mixing in a flow of variable CO₂ (Airgas, Bone Dry Grade) mixing ratios before sampling. At nominally 0 ppmv CO₂, the O_3^- ionization product (-48 m/Q) was

detected with sensitivity of 14 ± 2 ncps pptv⁻¹ and the CO₃⁻ product (-60 m/Q) at 5 ± 1 ncps pptv⁻¹. For CO₂ mixing ratios from 60 to 500 ppmv, the O₃⁻ signal is less than 1% of the CO₃⁻ product and the sensitivity at the CO₃⁻ product is independent of CO₂ within the uncertainty. The presence of a significant fraction (36%) of the CO₃⁻ product with nominally 0 ppmv CO₂ suggests the presence of a slight leak rate of CO₂ *via* diffusion through the perfluoroalkoxy alkane (PFA) tubing, or CO₂ contamination in the UHP N₂ supply. The manufacturer stated upper limit of CO₂ in the UHP N₂ is 1 ppmv which we take to be the lower limit achievable in our system. A CO₂ mixing ratio of only 1 ppmv is still an order of magnitude excess relative to a high end ambient O₃ mixing ratio of 100 ppbv. An exponential fit of the O₃⁻ product *vs* CO₂ indicates that O₃⁻ makes up less than 1% of the detected ozone at CO₂ mixing ratios greater than 10 ppmv. This suggests ambient samples will always have a substantial excess of CO₂ necessary to drive the reaction completely to the CO₃⁻ product. The measured flat response from 60–500 ppmv CO₂ indicates that natural variability in ambient CO₂ will have negligible impact on ambient measurements of ozone. No other analytes that we have calibrated for analyzed with the Ox-CIMS (HCOOH, HNO₃, H₂O₂) have shown a CO₂ mixing ratio dependence, demonstrating suggesting that CO₂ may be uniquely involved in the detection of O₃⁻ mechanism and is not a general feature of the oxygen-anion chemistry. All other reported laboratory calibrations reported here were performed at CO₂ mixing ratios of 380 ppmv and all reported sensitivities are for the CO₃⁻ product. This CO₂ dependence also requires careful consideration during instrument background determinations by UHP N₂ overflow which is discussed in Section 2.8.

2.7 Dependence on IMR pressure

Instrument sensitivity to O₃ increases with increasing IMR pressure as shown in Fig. 5. The normalized signal of O₃ increases by 17560% at an IMR pressure of 95 mbar compared to 70 mbar over the pressure range of 70 to 95 mbar in the IMR when sampling a constant O₃ source of 35 ppbv. IMR pressure was increased in approximately 5 mbar steps, with CDC pressure held constant at 2 mbar, and a three-minute dwell time at each step to ensure signal and pressure were stabilized. Total reagent ion signal did not change significantly over this pressure range. Pressures above 95 mbar were not investigated due to concerns over corresponding increases in CDC pressure with the pinhole and pumping configuration used in this work. There is no evident plateauing in the signal increase over the IMR pressure range investigated here, indicating that further optimization is likely possible by operating at higher IMR pressures. The increase in sensitivity with IMR pressure could be fit well with an exponential least squares fit, which is plotted in Fig.5. The physical meaning of the exponential relationship is not clear. The source of the response of sensitivity to pressure is not definitive but can possibly be attributed to the increase in the total number of collisions during the 100 ms residence time in the IMR and the corresponding weakening of those collisions. Higher collisional frequencies also lead to proportionally weaker collisions which could better preserve a weakly bound O₂(O₃)(H₂O)_n⁻ cluster and allow a longer lifetime to react with CO₂ before dissociation. The operational IMR pressure of 95 mbar used here was empirically selected to maximize sensitivity to O₃ without increasing CDC pressure beyond the desired

range. Investigation of higher IMR pressures, up to the operation of an atmospheric pressure interface, has the potential to further increase the instrument sensitivity to O₃.

2.8 Instrument background and limits of detection

255 Instrument backgrounds were assessed by periodically overflowing the inlet with UHP N₂ during field sampling. Details of the inlet and zeroing conditions used are discussed further in Section 3.1. During N₂ overflow, O₃ displayed a consistently elevated background on the order of 3.1×10^5 cps corresponding to 2.1×10^4 ncps, or approximately 1.3 ppbv O₃, at a typical total reagent ion signal of 1.45×10^7 cps. A representative background determination is shown in Fig. 6. The magnitude of the O₃ background was observed to vary with the O₂:N₂ ratio in the reagent ion precursor flow when sampling a UHP ZA overflow
260 with 380ppm CO₂ as shown in Fig. S2. The background O₃ count rate was observed to increase from 3.0×10^4 to 6.3×10^4 ncps as the O₂ volume fraction in the reagent ion delivery gas flow (f_{O_2}) was increased from 0.05 to 0.4. The dependence of the background O₃ signal on f_{O_2} suggests that the observed background O₃ is formed directly in the alpha ion source and is not from off-gassing of inlet and instrument surfaces. The magnitude of this background O₃ does not vary when sampling UHP zero air or N₂, further confirming that the background O₃ is formed directly in the ion source from the O₂ used to generate the
265 reagent ion. An operational f_{O_2} of 0.08 (actual volumetric flow ratio O₂:N₂ of 200:2200 sccm) was selected to balance maximizing the total reagent ion signal while minimizing the O₃ ion-source background (3.1×10^5 cps). The magnitude of this O₃ background was observed to be highly consistent during field sampling at a constant f_{O_2} of 0.08 and well resolved from all ambient observations (Fig. S3). The 1 σ deviation of the distribution of normalized adjacent differences of O₃ signal during background periods gives an upper limit of variability of 9% between adjacent background periods. A variability of 9%
270 corresponds to a difference of 70 pptv between subsequent O₃ background determinations. The magnitude of this O₃ background is a fundamental limit on the achievable limit of detection.

Because CO₂ was not added to the UHP N₂ overflow during field sampling, the reaction was not driven fully to the CO₃⁻ product and some O₃⁻ signal at $-m/Q$ 48 was observed during UHP N₂ overflow periods as shown in Fig. S4. The magnitude of the O₃ signal observed as O₃⁻ was approximately 55% of the CO₃⁻ product (mean 1.2×10^4 and 9.6×10^3 ncps
275 respectively) during overflow periods. The total sensitivity to O₃ as the sum of the O₃⁻ and CO₃⁻ was observed to be constant as a function of CO₂ as shown in Fig. 4. We therefore assign equal sensitivity to each O₃ detection product and took the sum of signal at O₃⁻ and CO₃⁻ in order to determine the total background O₃ concentration. This issue will be corrected in future deployments by the addition of CO₂ to the N₂ overflow used for backgrounds which will drive the product fully to CO₃⁻. The mean background of O₃ for the full field sampling period was 1.3 ± 0.3 ppbv. The 10 Hz precision of O₃ during an individual
280 N₂ overflow period was found to be 0.75%, corresponding to 7.5 pptv as shown in Fig. S5. This suggests that variability in the O₃ signal from this background source is constant over short timescales and has a negligible impact on instrument precision during ambient sampling.

The 10 Hz limit of detection for O₃ is 42 pptv for a S/N of 3, and a mean background O₃ signal of 2.1 x 10⁴ ncps as calculated using Eq. 1, below from Bertram et al., 2011, where C_f is the calibration factor, [x] is the analyte mixing ratio, t is averaging time in seconds, and B is the background count rate. The optimum LOD from the minimum of the Allan variance at an 11 second averaging time is 4.0 pptv (Fig. S6a).

$$\frac{S}{N} = \frac{C_f[X]t}{\sqrt{C_f[X]t - 2Bt}} \quad \text{E1}$$

The mean background signal during field sampling for NO₂ was 3.5 x 10³ ncps which corresponds to 0.28 ppbv. At this background level, the 10 Hz LOD for NO₂ is 26 pptv for a S/N of 3. The optimum LOD for NO₂ is 2.3 pptv at an averaging time of 19 seconds, determined from the minimum of the Allan variance (Fig. S6b). The background signal of NO₂ is notably above zero indicating either off gassing from inlet walls or a secondary production of NO₂ in the instrument. A possible source of this background is from degradation of other species such as nitric acid or alkyl nitrates on the inlet walls. Additional calibration ~~would~~will be necessary to ensure that observed NO₂ signal is not a secondary product of other species and we can currently quantify their potential interference on measured NO₂.

2.9 Reagent ion saturation and secondary ion chemistry

During ambient sampling the ozone signal (as CO₃⁻ detected at -60 m/Q) is of comparable magnitude to the O₂⁻ reagent ion signal as shown in Fig. 1. High analyte concentrations (> 5 ppbv) have been shown previously to result in non-linear calibration curves for unnormalized signals (Bertram et al., 2011; Veres et al., 2008). In our system we do not observe non-linearity in the normalized O₃ calibration for our highest concentration calibration point of 80 ppbv despite the CO₃⁻ signal being larger than the O₂⁻ reagent ion (9 x 10⁶ cps and 6 x 10⁶ cps respectively). The electron affinity (E.A.) of carbonate is from 3.26 (Hunton et al., 1985) to >3.34 eV (Snodgrass et al., 1990) and is significantly higher than that of oxygen (E.A. 0.45 eV), making it unlikely that carbonate is involved in charge transfer reactions when excess O₂⁻ is present. . At high O₃ concentrations, the reagent ion signal magnitude is reduced, which necessitates normalizing sensitivities to the 1 x 10⁶ cps of reagent ion signal before quantification. For NO₂ (E.A. 2.27 eV), the normalized sensitivity showed no dependence on O₃ concentrations from 0 to 80 ppbv. Carbonate reagent ion chemistry has been utilized for detection of HNO₃ and H₂O₂ *via* adduct formation raising additional concern about potential secondary ion chemistry (Reiner et al., 1998). In laboratory calibrations, shown in Fig. S7, introduction of 0 to 40 ppb H₂O₂ resulted in the titration of the O₃ signal of 0.06 ppbv per ppbv H₂O₂. H₂O₂ was detected as an adduct with O₂⁻ and not CO₃⁻, indicating that O₂⁻ reagent ion chemistry is more favorable despite high CO₃⁻ signal intensity. The Ox-CIMS O₃ measurement also compared well (R² = 0.99) against an EPA AQS O₃ monitor over 1 month of ambient sampling where H₂O₂ and HNO₃ concentrations both exceeded 5 ppbv at times (see Section 3.1 for further discussion of field intercomparison), further supporting the CO₃⁻ detection product as a robust indicator of O₃ in complex sampling environments.

Ab initio calculations of the binding enthalpies of O₂⁻ and CO₃⁻ reagent ions with H₂O, HNO₃, H₂O₂, and CH₃OOH were performed with the MP2/aug-cc-pvdz-PP theory and basis set in order to assess the relative favorability of adduct

315 formation between O_2^- and CO_3^- Adduct formation with O_2^- was favorable relative to CO_3^- by 2.5 to 17 kcal mol⁻¹ for all analytes that were calculated. All calculated binding enthalpy values are listed in Table S2.

2.10 Reagent ion saturation and secondary ion chemistry Short- and long- term precision

Short term precision of the instrument was assessed by calculating the normalized difference between adjacent 10 Hz data points over a 27-minute sampling period of a constant ambient analyte concentration *via* Eq. 2.

$$NAD = \frac{|X|_n - |X|_{n-1}}{\sqrt{|X|_n |X|_{n-1}}} \quad E2$$

320 The standard deviation of the Gaussian fit of the distribution of normalized adjacent differences (NAD) is a direct measure of the short-term instrument precision (Bertram et al., 2011). The 1 σ precision from the NAD distribution for 10 Hz sampling of 38 ppbv ozone is 0.74% (Fig. 7). The 10 Hz precision for sampling of 2.3 ppbv NO₂ is 1.1% The short-term precision for both analytes was larger than expected if the noise was driven by counting noise alone (10 Hz counting noise limit for O₃ and NO₂ at the concentrations used above are 0.12% and 0.63% respectively), indicating that other potential points of optimization in
325 the instrument configuration are required to further improve short-term precision. Notably, the observed noise source appears to be white noise given the Gaussian distribution of the NAD (Thornton et al., 2002b).

Short term precision was assessed as a function of count rate by calculating the NAD for all masses in the spectrum over a stable 27-minute sampling period for both 1 Hz and 10 Hz data averaging. From this assessment, precision was observed
330 to improve approximately linearly in a log-log scaling for count rates between 1 x 10³ and 1 x 10⁶ cps (Fig. S8) as expected in the case where counting noise drives instrument precision. Above 1 x 10⁶ cps there is an apparent asymptote where precision no longer improves with count rate. ~~For 10 Hz averaging and count rates of 1 x 10⁶ and 1 x 10⁷ cps, the corresponding instrument precision is 0.75 and 2% respectively, and appears independent of count rate.~~ The counting noise limited 10 Hz precision for 10⁶ and 10⁷ cps ~~are~~ 0.32% and 0.1% respectively, while the measured values were 0.75 and 2%. The counting noise limited precision is calculated as \sqrt{N}/N where N is the number of counts during the integration time. This precision limit
335 could be driven by an uncharacterized source of white noise in the instrument, including MFC drift, IMR turbulence, ion optic voltage drift, and pump drift. Measurement precision of O₃ and NO₂ could be improved by a factor of 5 and 2 respectively if this non-counting noise source of white noise was eliminated.

In theory, detection limits can be improved by signal averaging to a lower time resolution than the 10 Hz save rate.
340 Signal-to-noise ratios are expected to improve with the square root of the integration time. At longer timescales, factors including instrument drift become significant, creating a limit on the upper end of averaging time which optimizes signal-to-noise. This was assessed quantitatively by calculation of the Allan variance as shown in Fig. S6 (Werle et al., 1993).

3 Field results and discussion

3.1 Ozone field calibration and intercomparison

345 Performance of the Ox-CIMS was compared against a co-located EPA Air Quality System (AQS) O₃ monitor (Thermo-Fisher
49i, AQS ID 17-097-1007) over one month of ambient sampling during the Lake Michigan Ozone Study 2017 (LMOS 2017)
in Zion, IL (Vermeuel et al., 2019). A regression analysis between the two instruments at one-minute averaging showed strong
agreement ($R^2 = 0.99$) as shown in Fig. 8. Ox-CIMS concentrations were averaged to 1 ppbv bins which was the output data
350 resolution of the EPA data logger system for the (Thermo-Fisher 49i). Error bars are the 1σ standard deviation of each Ox-
CIMS bin average. Near one-to-one agreement (slope of 0.99) between instruments lends confidence to the calibration,
baselining, and long-term stability of the Ox-CIMS. [The Ox-CIMS was located on the roof of a trailer \(approx. 5 m above
ground\) and sampled through a 0.7 m long, 0.925 cm i.d., PFA inlet. The inlet was pumped at flow rate of 18-20 slpm from
which the Ox-CIMS subsampled at 1.5 slpm. Temperature and RH were recorded inline downstream of the subsampling point.
The Ox-CIMS sampling point was approximately 10 m horizontally from the Thermo-Fisher 49i and both instruments sampled
355 at approximately equal heights. Instrument backgrounds of the Ox-CIMS were determined every 70 minutes by
overflowing the inlet with dry UHP N₂. Calibration factors for O₃ were determined by sealing by the in-field continuous
addition of a C-13 isotopically labelled formic acid standard to the tip of the inlet. Laboratory calibrations of the Ox-CIMS to
formic acid and O₃ as a function of specific humidity were determined immediately pre- and post-campaign and were used to
calculate a humidity dependent sensitivity of O₃ relative to formic acid. That relative sensitivity was then used to determine
360 the in-field sensitivity to O₃ by scaling field sensitivities of formic acid from the continuous additions to humidity dependent
calibration factors for O₃ and formic acid determined in lab pre- and post-campaign as. Full details of this deployment and
calibration methods are described in Vermeuel et al., \(2019\). The EPA O₃ monitor shows a persistent high bias at low O₃
concentrations \(<10 ppbv\) relative to the Ox-CIMS. This discrepancy could arise from known interferences from water,
mercury, and other species in 254 nm UV absorbance detection of ozone \(Kleindienst et al., 1993\).](#)

365 3.2 Eddy covariance experiment overview

The Ox-CIMS was deployed to the 330 m long Ellen Browning Scripps Memorial Pier (hereon referred to as Scripps Pier) at
the Scripps Institute of Oceanography (32° 52.0' N, 117° 15.4' W) during July and August 2018 for EC measurements of O₃
vertical fluxes. This site has been used regularly for EC flux observations from our group and others (Ikawa and Oechel, 2015;
Kim et al., 2014; Porter et al., 2018). The Ox-CIMS was housed in a temperature-controlled trailer at the end of the pier. The
370 Ox-CIMS sampled from a 20 m long PFA inlet manifold with the intake point co-located with a Gil-Sonic HS-50 sonic
anemometer which recorded 3-dimensional winds sampling at 10 Hz. The Ox-CIMS inlet and sonic anemometer were mounted
on a 6.1 m long boom that extended beyond the end of the pier to minimize flow distortions. The inlet height was 13 m above
the mean lower low tide level. The Ox-CIMS inlet was located 8 cm below the sonic anemometer with a 0 cm horizontal
displacement. The inlet manifold consisted of a 0.64 cm i.d. sampling line, a 0.64 cm i.d. overflow line, and a 0.47 cm i.d.

375 calibration line all made of PFA. The inlet sample line was pumped at 18-23 slpm (Reynolds number 3860-4940) by a dry
scroll pump (SH-110, Agilent) to ensure a fast time response and maintain turbulent flow. Flow rates in the inlet sample line
were recorded by a mass flow meter but were not actively controlled. The inlet manifold, including calibration and overflow
lines, was held at 40 °C *via* a single resistively coupled circuit along the length of the manifold and controlled by a PID
380 controller (Omega, model CNi 16). The Ox-CIMS front block and IMR were held at 35 °C. The Ox-CIMS subsampled 1.5
slpm from this inlet manifold through a critical orifice into the IMR. Ambient humidity and temperature were also recorded
in-line downstream of the subsampling point.

3.2.1 Calibration

Instrument sensitivity was assessed by the standard addition of a C-13 isotopically labelled formic acid standard for 3 minutes
every 35 minutes at the ambient end of the inlet manifold. Ozone mixing ratios were determined by scaling the humidity
385 dependent sensitivity of O₃ from pre- and post-campaign calibrations to the field calibrations of C-13 formic acid. Ambient
O₃ was also measured at 10 s time-resolution with a 2B technologies Personal Ozone Monitor (POM). The POM had a separate
10 m long, 0.47 cm i.d. PFA sampling line located 12 m from the Ox-CIMS inlet manifold and sonic anemometer. The POM
was used as an independent verification of the Ox-CIMS measurement and was not used for calibration.

3.2.2 Backgrounds and inlet residence time

390 Instrument backgrounds were determined every 35 minutes by overflowing the entire inlet manifold with dry UHP N₂.
Background and ambient count rates were first converted to concentrations using the laboratory determined humidity
dependent sensitivities for O₃ and NO₂ scaled to the C-13 formic acid standard addition sensitivity. Background concentrations
of O₃ and NO₂ from before and after each 30-minute ambient sampling period were interpolated over the ambient sampling
period which was then subtracted from each 10 Hz concentration data point to obtain a background corrected time-series.
395 Background concentrations of O₃ had a mean 1.5 ppbv and a drift of 1% between adjacent background periods, determined by
the distribution of the NAD of the mean background concentrations.

The signal response of O₃ during dry N₂ overflows were fit to an ~~bi~~-exponential decay function to characterize inlet
gas ~~response times~~ ~~evacuation time (τ_1) and wall interaction times (τ_2)~~ (Ellis et al., 2010). Best fit estimates for ~~decay time~~
~~constants τ_1 for~~ O₃ and NO₂ across overflow periods were from 0.27 to 0.44-1.2 seconds ~~and accounted for more than 80% of~~
400 ~~the decay. For O₃, τ_2 was found to be negligible at less than 0.3 s indicating O₃ has minimal equilibration with the inlet walls.~~
~~NO₂ decay responses were fit to a bi-exponential decay to characterize inlet evacuation time (τ_1) and wall interaction times~~
~~(τ_2) (Ellis et al., 2010). τ_2 for NO₂ was determined to be approximately longer at 3.2 s. This suggests a potential interference at~~
405 ~~the NO₂ peak, as NO₂ is expected to have minimal wall equilibration, similar to O₃. NO₂ also shows a continually elevated~~
~~signal during overflow periods suggesting off gassing from inlet or instrument surfaces. The cause of this slow NO₂ decay and~~
~~elevated background is not clear but could be from degradation of nitric acid or nitrate containing aerosol on the instrument~~
~~surfaces.~~

The instrument response time (τ_r) for O_3 can be calculated during zeroing periods as the time required for the signal to fall to 1/e of its initial value. The response time of the instrument was calculated for each overflow period during field sampling, with a mean value of 0.289 s. The cutoff frequency (f_{cut}) of the instrument is defined as the frequency where the signal is attenuated by a factor of $1/\sqrt{2}$ (Bariteau et al., 2010). The cutoff frequency can also be calculated from τ_r according to Eq. 3.

$$f_{cut} = \frac{1}{2\pi\tau_r} \quad \text{E3}$$

The calculated f_{cut} from the measured mean response time was 0.5748 Hz. This value suggests that minimal attenuation in the flux signal (cospectra) should be apparent at frequencies less than 0.5748 Hz. The instrument response time and thus cutoff frequency are function of the flow rate and sampling line volume. The flow rate of 18-23 slpm was the maximum achievable with the tubing and pumping configuration used here but could be improved in future to minimize tubing interactions and shift f_{cut} towards higher frequencies.

3.2.3 Eddy covariance flux method

The transfer of trace gases across the air–sea interface is a complex function of both atmospheric and oceanic processes, where gas exchange is controlled by turbulence in the atmospheric and water boundary layers, molecular diffusion in the interfacial regions surrounding the air–water interface, and the solubility and chemical reactivity of the gas in the molecular sublayer. The flux (F) of trace gas across the interface is described by Eq. 4, as a function of both the gas-phase (C_g) and liquid phase (C_l) concentrations and the dimensionless gas over liquid Henry’s law constant (HK_H), where K_t , the total transfer velocity for the gas (with units cm s^{-1}), encompasses all of the chemical and physical processes that govern air–sea gas exchange. Surface chemical reactivity terms to the gas exchange rate are incorporated into the K_t term.

$$F = -K_t(C_g - HK_H C_l) \quad \text{E4}$$

Trace gas flux (F) can be measured with the well-established eddy covariance (EC) technique where flux is defined as the time average of the instantaneous covariances from the mean of vertical wind (w) and the scalar magnitude (here O_3) shown in Eq. 5. Overbars are means and primes are the instantaneous variance from the mean. Here N is the total number of 10 Hz data points during the 27-minute flux averaging period.

$$F = \frac{1}{N} \sum_{i=1}^N (w_i - \bar{w})(O_{3,i} - \bar{O}_3) = \langle w'O_3' \rangle \quad \text{E5}$$

$$v_d = \frac{F}{\bar{C}_g} \quad \text{E6}$$

For purely depositing species where the water side concentration is negligible, C_l and HK_H can be neglected in Eq. 4 and K_t can be reformulated into a deposition velocity (v_d) calculated according to Eq. 6, where \bar{C}_g is the mean gas phase mixing ratio during the flux averaging period. A summary of concentration and flux results for the full deployment period are given in Table 2.

3.3 General Data Corrections

Several standard eddy covariance data filters and quality control checks were applied before analysis. General filters included:

- 1.) Wind sector: Only periods of mean onshore flow (true wind direction 200-360°) were used.
- 2.) Friction velocity: A friction velocity (U_*) threshold of 0.1 m s^{-1} was applied to reject periods of low shear driven turbulence (Barr et al., 2013) [described further below](#).
- 3.) Stationarity: Each 27-minute flux period was divided into five even non-overlapping subperiods. Flux periods were rejected if any of the subperiods differed by more than 40% (Foken and Wichura, 1996).

The ~~applied~~ selected U_* threshold filter was determined by comparing the observed U_* values to U_* calculated with the [NOAA COARE bulk flux v 3.6 algorithm](#) (Fairall et al., 2011). [COARE \$U_*\$ were calculated using measured meteorology including wind speed, sea-surface temperature, air temperature, and relative humidity. Flux periods were rejected if the observed \$U_*\$ differed from the calculated \$U_*\$ by more than 50%. The stress relationship of wind-speed to \$U_*\$ is well understood over the ocean. Fixed \$U_*\$ filters of *ca.* of \$0.1 \text{ m s}^{-1}\$ is lower than the \$0.2 \text{ m s}^{-1}\$ are used frequently as a default in terrestrial flux studies but would reject nearly all observation periods in this study.](#) ~~but is~~ [The observed friction velocities are](#) consistent with other marine flux studies where surface roughness lengths are significantly smaller than over terrestrial surfaces (Porter et al., 2018). Methods of determining site specific U_* thresholds typically require long-term data series which were not available here (Papale et al., 2006). Papale et al., (2006), applied a minimum U_* threshold of 0.1 m s^{-1} for forest sites and 0.01 m s^{-1} for short vegetation sites where typical U_* values are lower. ~~A default U_* of 0.2 m s^{-1} , which is a common value selected for terrestrial environments would reject over 80% of flux periods from our data set.~~ The selected U_* filter ~~rejects an additional~~ [sults in 44.57% of the flux periods remaining after the wind direction filter.](#) ~~ed flux periods being rejected.~~ [The stationarity criteria rejected a further 100 flux periods, potentially driven by periods of activity on the pier driving changes in the sampled \$O_3\$. Outliers in \$v_d\(O_3\)\$ and the flux limit of detection were determined and removed for points three scaled median absolute deviations from the median.](#) ~~Outliers in $v_d(O_3)$ and the flux limit of detection were determined and removed for points three scaled median absolute deviations from the median.~~ This outlier filter removed an additional 164 data points. After [the wind direction filter and](#) all quality control filters were applied, [73.84%](#) of flux periods were rejected leaving [157-246](#) quality-controlled flux periods. Eddy covariance flux values were calculated using 27-minute time windows. The O_3 timeseries was detrended with a linear function prior to the flux calculation. The O_3 and vertical wind data were despiked using a mean absolute deviation filter before the eddy covariance flux calculation following Mauder et al., (2013).

3.3.1 Planar Fit Wind Coordinate Rotation

Coordinate rotation of the u , v , and w wind components was performed by the planar fit method to remove unintentional tilts in the sonic mounting and account for local flow distortions (Wilczak et al., 2001). Briefly, the mean u , v , and w wind components and the stress tensor were determined for each 15-minute onshore flow period during the full campaign. A linear

regression was used to find the best fit of a plane with a coordinate system where the z-axis is perpendicular to the mean
470 streamline. Individual 27-minute flux periods are then rotated such that the x-axis is along the mean wind and $\bar{v} = 0$. Vertical
wind velocity (\bar{w}) in any individual rotation period may be non-zero due to mesoscale motions but \bar{w} for the full campaign is
zero. The residual mean vertical velocity in any individual rotation period is subtracted out, so it does not impact the Reynolds
averaging.

3.3.2 Lag time shift

475 The Ox-CIMS signal is delayed relative to the sonic anemometer due to transit time in the inlet line which must be accounted
for before calculating the covariance between the vertical wind and analyte concentration. The cross-covariance of the two
timeseries were first calculated within a ± 5 s window to determine the lag time of the Ox-CIMS and synchronize with the
anemometer. The volumetric evacuation time of the inlet is 1.65 to 2.1 s for the inlet volume and flow rates of 18 to 23 slpm
used in this study. Following the method and terminology outlined in Langford et al., (2015), the position of the maximum
480 (MAX) of the cross-covariance is taken as the lag time needed to align the vertical wind and analyte concentration for that flux
period. A representative lag time determination with a larger lag window (± 10 s) using the MAX method is shown in Fig. 10.
In low signal-to-noise (SNR) data, the use of the MAX leads to high variability in the determined lag time caused by uncertainty
in the position of the peak in the cross-covariance. This results in a systematic high bias on the absolute magnitude of the
resulting flux. The position of the maximum of a centered running median (AVG) function of the cross-covariance is an
485 alternative method to determine lag time with less expected bias for low SNR data (Langford et al., 2015; Taipale et al., 2010).
Lag times for each O_3 flux period determined by the MAX and a 10 point AVG method showed reasonable agreement, with a
campaign average lag time from the MAX with a mean of 1.0 seconds and the AVG at 0.7 seconds (Fig. S9). This agreement
suggests that a clear peak in the cross-covariance was present for most flux periods leading to a convergence of the two
methods. This lag time also shows agreement with the inlet response time of 0.9 s determined during dry N_2 overflows. Due
490 to the convergence of the determined lag times around a central value, a prescribed lag time of 0.9 s was used for all reported
 $v_d(O_3)$ values. A prescribed lag time has the least bias to extreme values caused by noise, provided that the true lag time is
known well (Langford et al., 2015). Deposition velocities were then recalculated with the prescribed lag time of 0.9 s and with
the MAX and AVG method over a narrower lag window of ± 3 which is expected to be physically reasonable range for the
flow rate and inlet line volume. The mean $v_d(O_3)$ using the prescribed, MAX, and AVG lag times were 0.0131, 0.0129, and
495 0.0129 $cm\ s^{-1}$ respectively, suggesting the campaign mean value was relatively insensitive to the lag time method.

3.4 Cospectra and Ogives

The frequency weighted cospectrum of O_3' with w' has a well characterized form with exhibited dependence on wind-speed
and measuring height (Kaimal et al., 1972). Comparison of observed cospectra shape against the idealized Kaimal cospectra
is useful to validate that the observed signal was not significantly attenuated at low or high frequencies. Cospectral averaging
500 is performed by binning frequency into 50 evenly log spaced bins and normalizing the integrated cospectra to 1. The integral

of the unnormalized cospectra is the flux for that observation period. The mean wind-speed binned cospectra of sensible heat and O₃ appear to match well with the idealized Kaimal cospectra for an unstable boundary layer at sampling height $z = 13\text{m}$ (Fig.11).

505 The ogive is the normalized cumulative distribution of the cospectra, which is used to validate both that no high-frequency attenuation is present and that the flux averaging time is sufficiently long that all frequencies contributing for the flux is captured. Figure 11 shows the averaged cospectra and ogives for O₃ and sensible heat flux from the average of two flux averaging periods 14:10 – 15:20 on July 20th. The asymptote to 1 at low frequencies validates that the 27-minute flux averaging time was sufficiently long for this site to capture the largest flux carrying eddies. High pumping rates in sampling line ensured
 510 that turbulent flow was always maintained in the line (Reynolds number 3860-4940). Higher Reynolds numbers in the turbulent regime lead to smaller high frequency attenuation (Massman, 1991). The overlap of the idealized Kaimal curve and the observed sensible heat and O₃ ogives suggest that high frequency attenuation in the sampling line is minimal above approximately 0.42 Hz, consistent with our calculated f_{cut} of 0.5748 Hz. ~~Due to the small magnitude of the O₃ EC flux there is low signal to noise in the cospectra at high frequency for many of the flux averaging periods. This makes application of~~
 515 ~~cospectra based correction factors challenging and likely to introduce added variance on the signal.~~ We calculate the high frequency correction transfer function for turbulent attenuation in a tube from Massman, (1991) as a constraint, which is shown in Fig. 11b. This transfer function shows attenuation primarily above 1 Hz and is not sufficient to describe the observed attenuation above 0.2-4 Hz. This implies that the attenuation observed cannot be explained only as turbulent smearing in the inlet and that other wall interactions are likely present.

520 ~~Due to the small magnitude of the O₃ EC flux there is low signal to noise in the cospectra at high frequency for many of the flux averaging periods. This makes application of cospectra based correction factors challenging and likely to introduce added variance on the signal. We therefore apply an attenuation correction factor following (Bariteau et al., (2010). First we calculate the idealized unattenuated Kaimal cospectra ($C_{wx,k}$) (Eq. 7) for each flux period, and then apply frequency attenuation to that cospectra by applying a low-pass filter function ($H(f)$) characterized by τ_c (Eq. 8). The ratio of the flux of the unattenuated (F_{raw}) and attenuated (F_{att}) cospectra is then taken as the correction factor (A_f , Eq.9) to apply to the observed O₃ flux (Eq. 10). Where n is the surface layer normalized frequency defined as $n = fz/U$, where z is the measurement height and U is the horizontal wind speed. $F_{O_3,corr}$ is the attenuation corrected O₃ flux and $F_{O_3,obs}$ is the original measured flux. This approach has the benefit of applying a single correction factor to the total flux, rather than frequency dependent corrections which might serve to amplify noise at high frequencies. The net impact of this correction factor was an increase of campaign mean $v_d(O_3)$~~
 525 ~~of 4%.~~

$$C_{wx,k} = \frac{11n}{(1+11.3n)^{7/4}} \quad \text{E7.}$$

$$H(f) = [1 + (2\pi f \tau_c)^2]^{-1} \quad \text{E8.}$$

$$A_f = \frac{F_{raw}}{F_{att}} \frac{\int_0^{f_n} c_{wxk}(f) df}{\int_0^{f_n} c_{wxk}(f) [H(f)]^{1/2} df} \quad \text{E9.}$$

$$535 \quad F_{O_3,corr} = A_f F_{O_3,obs} \quad \text{E10.}$$

We also calculate the attenuated flux from the model of Horst, (1997) shown in Eq. 711, for a response time (τ_c) of 0.9-0.28 s, and a wind speed of 3 m s⁻¹ to be 643%. The general agreement of the Horst and Bariteau attenuation correction factors indicate that the applied correction is reasonable.

$$540 \quad \frac{F_m}{F_x} = \frac{1}{1+(2\pi n_m \tau_c U/z)^\alpha} \quad \text{E7E11}$$

Where F_m/F_x is the ratio of the measured flux to the unattenuated flux, U is wind speed, z is measurement height, and n_m and α are scaling factors for an unstable boundary layer taken as 0.085 and 7/8 respectively. ~~This flux attenuation of 13% is in reasonable agreement with the attenuation visible in the ogives shown. Given the uncertainty in the eospectra at high frequencies it is difficult to make a quantitative statement as to whether the observed attenuation is consistent throughout the measurement period. We therefore elect to report the uncorrected flux value here while acknowledging they are potentially a lower estimate with reasonable correction factors on the order of 15%.~~

3.5 Uncertainty and flux limit of detection

Variance in the atmospheric O₃ signal was estimated by calculating the autocovariance of the signal during a 27-minute flux averaging period (Fig. S11). Uncorrelated white noise only contributes to the first point in the autocovariance spectrum, while autocovariance at longer time shifts represents real atmospheric variance or correlated instrument drift (Blomquist et al., 2010; Langford et al., 2015). For the analysed period, white noise is typically 45 to 65% of the total variance and atmospheric variance is 35 to 55%. This corresponds to a standard deviation from white noise $\sigma_{O_3, noise}$ of 0.4 ppbv.

The error in each flux averaging period (LOD_σ) can be determined by taking the standard deviation of the cross-covariance between vertical wind speed and mass spectrometer signal at lag times significantly longer than the calculated true lag time (Spirig et al., 2005; Wienhold et al., 1995). The random flux error is determined using lag windows of -150 to -180 and 150 to 180 s, which are significantly larger than the true lag time from sensor separation of 0.9 s as shown in Figure S12. The selection of the -150 to -180 and 150 to 180 s lag windows is somewhat arbitrary and may still capture organized atmospheric structure that persists over long time periods. We also calculate the root mean squared deviation (LOD_{RMSE}) of the cross-covariance over the same lag windows as proposed by Langford et al., (2015), which captures the variance in the cross-covariance in those regions but also accounts for long term offsets from zero in the cross-covariance. The resulting error from the LOD_σ and LOD_{RMSE} methods showed good correlation (Fig S13), with periods where the LOD_{RMSE} error is larger. We apply the RMSE method for our reported flux error determination. The final deposition velocity limit of detection was determined for each 27-minute flux averaging period by multiplying the LOD_{RMSE} error by 1.96 to give the flux limit-of-

565 detection at the 95% confidence level. The flux error was then divided by the mean O₃ concentration for that averaging period
to convert from flux to deposition velocity units. The campaign ensemble flux LOD_{RMSE} was 0.002742 cm s⁻¹, calculated using
Eq. 128 following Langford et al.,(2015). A total of 5962 out of 246157 (2439%) flux periods had deposition velocities below
the campaign ensemble LOD. These values are still included in the reported mean $v_d(O_3)$.

$$\overline{LOD} = \frac{1}{N} \sum_{i=1}^N LOD^2 \quad E128$$

570 3.6 Density fluctuation corrections

The Ox-CIMS measures O₃ as the apparent mixing ratio relative to moist air, as is true of all CIMS based measurements, which
means fluctuations in the density of air due to changes in temperature, pressure, and humidity could introduce a bias in the EC
flux measurement (Webb et al., 1980). The temperature and pressure in the Ox-CIMS and sampling lines were both actively
controlled during sampling, making density fluctuations from those sources negligible. The long (20 m) inlet sampling line
575 used likely also dampened a substantial portion of the water vapor flux. This has been demonstrated in an EC study utilizing
a closed path H₂O sensor for EC flux measurements (through an 18 m long, 0.635 cm i.d. inlet, pumped at 18 slpm, comparable
to the inlet used in this study) which showed complete attenuation above 0.1 Hz and overall attenuation of ~80% of the H₂O
(latent heat) flux (Yang et al., 2016). However, without a direct measure of water vapor fluctuations collocated with the Ox-
CIMS this is difficult to assess directly definitively rule out in our measurement. We therefore calculate a conservative estimate
580 of this correction factor from Eq 45b. in Webb et al., (1980), assuming a latent heat flux of 50 W m⁻² and neglecting the
sensible heat term which is removed by active heating of the inlet which is removed by active heating of the inlet. For a specific
humidity of 12 g kg⁻¹, a temperature of 293 K, a pressure of 1 atm, and an O₃ mixing ratio of 40 ppbv, we calculate a flux
correction term of 2.6 x 10⁹ molecules cm⁻² s⁻¹, which is 2024% of our mean measured flux of -1.34 x 10¹⁰ molecules cm⁻² s⁻¹.
We expect that the actual density correction for our instrument much smaller given that water vapor fluctuations were likely
585 dampened in the inlet line, and the high latent heat flux used in the calculation (50 W m⁻²). Due to the uncertainty in this
correction term for our instrument, we do not add it to our measured flux values and instead use the calculated value above as
a conservative constraint on the magnitude. The addition of a Nafion drier on the inlet has been successfully implemented in
other O₃ flux instruments to fully remove water fluctuations and will be used in future deployments of the Ox-CIMS (Bariteau
et al., 2010).

590 3.7 Flux divergence

3.7.1 Surface NO emissions

The observed dry deposition velocity of ozone is potentially biased by simultaneous air-sea exchange of nitric oxide (NO).
NO is expected to be emitted from the ocean on the order of 1 x 10⁸ molecules cm⁻² s⁻¹ with dependence on dissolved surface
nitrate and solar irradiance (Zafirou and McFarland, 1981). This NO source near the surface will cause titration of O₃ to NO₂
595 resulting in a positive bias for the observed $v_d(O_3)$. Assuming a maximum NO emission flux of 5 x 10⁸ molecules cm⁻² s⁻¹ and

that all NO reacts with O₃ before being advected to the sensor height, the resulting O₃ flux bias would be -5 x 10⁸ molecules cm⁻² s⁻¹. Our mean case of 40 ppbv O₃ and v_d (O₃) of 0.0134 cm s⁻¹ corresponds to a flux of -1.34 x 10¹⁰ molecules cm⁻² s⁻¹. Therefore, the resulting bias in observed v_d (O₃) from NO emissions is 34.85% or 4.949 x 10⁻⁴ cm s⁻¹. This value is an upper limit for expected ocean NO emissions and is well within the uncertainty of the observed v_d (O₃). There is also potential for short term anthropogenic emissions of NO (such as from a boat engine passing by the sensor) to create a flux divergence term. We expect that the combination of signal despiking and the flux stationarity criteria described in Section 3.3 will minimize the impact of this potential divergence term. Despiking will remove most short term (<1 s) emission events and the stationarity criteria will filter out any period where longer term titration events cause large changes in the observed flux within a flux measurement period.

605 3.7.2 Free troposphere entrainment

The entrainment of O₃ enhanced or depleted air in the free troposphere to the marine boundary layer (MBL) creates a potential flux gradient that will contribute to the measured flux values at the near surface measurement height (z_o) of 13 m. (Lenschow et al., (1982) presented aircraft observations of O₃ deposition over the Gulf of Mexico at heights of 15, 60, and 325 m which showed a strong flux gradient term driven by entrainment from the free troposphere. The boundary layer height (z_i) during those flights was approximately 1.2 km, suggests a strong flux gradient was present even within the surface layer (approximated as the lowest 10% of the boundary layer). The magnitude of this flux gradient depends on the magnitude of the O₃ concentration gradient (ΔC) and the entrainment velocity (w_e) of air from free troposphere into the MBL. Faloon et al., (2005), reported entrainment velocities from 0.12 to 0.72 cm s⁻¹ and an enhancement in O₃ (ΔC) of 20 ppbv in the free troposphere relative to the boundary layer in the summertime eastern subtropical pacific. Using those values and Equations 9

610 13 and 10-14 below we calculate the percent fractional error from entrainment on the observed flux for a range of reasonable ΔC and w_e as shown in Fig. 12 (Blomquist et al., 2010).

$$\frac{\Delta F_{0,est}}{F_0} = \frac{z}{z_i} \left(\frac{F_i}{F_0} - 1 \right) \quad \text{E139}$$

$$F_i = w_e \Delta C \quad \text{E140}$$

Where z_i is the boundary layer height, z_o is the measurement height, and F_i and F_0 are the entrainment flux and surface flux respectively. We use the SIO measurement height (z_o) = 13 m and mean surface flux (F_0) = -5.244 x 10⁻³ ppbv m s⁻¹ (from v_d = 0.0134 cm s⁻¹ and [O₃] = 40 ppbv), and an O₃ mixing ratio gradient (ΔC) from -20 to +20 ppbv in the free troposphere relative to the boundary layer. The resulting fractional error in our observed mean surface flux from Scripps Pier using the values from Faloon et al, 2005 (ΔC of +20 ppbv, MBL height of 800m) is 4.4625% for w_e of 0.12 and 3344% for 0.72 cm s⁻¹. This entrainment flux error is clearly significant for marine O₃ flux measurements assuming there is a gradient of O₃ in the free troposphere relative to boundary layer. This entrainment flux error is independent of the surface flux instrument measurement error and adds a systematic bias on the surface flux measurement. This calculation also makes clear that marine O₃ measurements should be made as close to the surface as possible, and that the O₃ concentration gradient and entrainment

rate should be explicitly measured if possible. We do not have an explicit measure of ΔC , w_e , or the MBL height so we tentatively assign entrainment error of up to 3344% from the maximum values of those parameters reported in Faloon et al. (2005). We emphasize this source of uncertainty is independent of the O₃ sensor and is a systematic bias that should be considered in all O₃ air-sea exchange determinations.

4 Fast NO₂ measurements, eddy covariance and O₃ titration

Discussion of EC flux results have been limited to O₃ because ocean-atmosphere exchange of NO₂ is expected to be small and below the limit of detection of our instrument. The potential flux divergence from the reaction of O₃ with NO is also below the instrument flux limit of detection as discussed in section 3.6. However, over terrestrial surfaces where NO₂ emissions can be large, we expect this instrument would be well suited for measuring NO₂ flux. From following Equations 15 and 16, following ~~in~~ Bariteau et al., (2010) and (Lenschow and Kristensen, (1985), we calculate the we calculate an expected flux LOD for the case where counting noise is the controlling term in the flux error. The calculated flux LOD is of 4.3 x 10⁹ molecules cm s⁻² s⁻¹ (1.6 pptv m s⁻¹) for an NO₂ mixing ratio of 1 ppbv and a friction velocity of 0.2 m s⁻¹.

$$F = C_a \sqrt{\frac{0.06 u_*^2}{C_a \xi \Gamma}} \quad \text{E15}$$

$$\Gamma = \frac{a z}{U} \quad \text{E16}$$

Where u_* is the friction velocity (m s⁻¹), C_a is the gas phase concentration (ppbv), ξ is the instrument sensitivity (cps ppbv⁻¹), and Γ is the integral time scale (s). Γ can be further expressed following Eq. 12 where a is constant taken as 0.3 for neutral conditions (Lenschow and Kristensen, 1985), z is the measurement height (here 10 m), and U is the horizontal wind speed at that measurement height (taken as 5 m s⁻¹).

Observations of a short duration NO plume from a boat motor starting near our inlet at Scripps Pier highlights the utility of the simultaneous O₃ and NO₂ detection from this instrument (Fig. 13). Highly localized NO emissions were observed as the titration of O₃ and prompt production of NO₂. Observed total odd oxygen (O_x = O₃ + NO₂) was conserved during this titration event, where NO₂ and O₃ concentrations were determined from independent calibration factors and backgrounds. The 1:1 conversion of O_x from O₃ to NO₂ shown in Fig. 13b, validates the laboratory generated instrument calibration factors for O₃ and NO₂. The temporal agreement of the O₃ and NO₂ signals also demonstrates that both O₃ and NO₂ are transmitted through the inlet and detected with nearly identical instrument response times. This analysis assumes that there were no direct NO₂ emissions during the titration event. A NO₂ to NO_x emission ratio of 0.08 was observed for ship emissions from diesel motors on inland shipping vessels (Kurtenbach et al., 2016). Without additional knowledge amount the NO_x emission source during this event, the observed conservation of total O_x could be partially driven by compensating errors within 10%. This simultaneous detection of both O_x species is likely also well suited for mobile sampling in the presence of dynamic NO

emission sources, which challenge other fast ozone measurements. This method would also be well suited for direct measurement of flux divergence in the presence of strong surface NO emission sources.

660 **5 Conclusions and Outlook**

This study demonstrated the utility of oxygen anion chemical ionization mass spectrometry for the fast and sensitive detection of O₃ and NO₂. Field measurements of O₃ dry deposition to the ocean surface from Scripps Pier, La Jolla CA demonstrate that this method has suitable time response, precision, and stability for successful EC measurements. The mean measured $v_d(\text{O}_3)$ with the Ox-CIMS is in ~~within range of good agreement with~~ prior studies of O₃ ocean-atmosphere exchange. Further
665 optimization and characterization of the Ox-CIMS is ongoing, including efforts to validate the specificity of the NO₂ detection, addition of a Nafion drier system, and better background determination methods. While this work has focused primarily on the deposition of O₃ to the ocean surface, the demonstrated instrument performance suggests the Ox-CIMS to be highly capable of O₃ and NO₂ flux measurements in the terrestrial biosphere and urban environments and from mobile platforms.

670 **Author Contributions**

GAN, MPV, and THB designed the lab and field experiments and GAN and MPV collected all data. GAN lead the data processing, interpretation and analysis with MPV contributing. GAN prepared the manuscript with contributions from all co-authors. THB supervised all work and contributed to data analysis, writing and editing of the manuscript.

Acknowledgments

675 This work was supported by National Science Foundation (NSF) Grant GEO AGS 1829667.

The authors thank the staff at Scripps Pier, Scripps Institute of Oceanography and at the UW—Madison Department of Limnology for support in instrument deployments.

Glenn M. Wolfe is gratefully acknowledged for publicly providing a Matlab based “FluxToolbox” of analysis scripts, portions of which were altered for use in this analysis. Code is archived at <https://github.com/AirChem>

680 This research was performed using the computing resources and assistance of the UW-Madison Center for High Throughput Computing (CHTC) in the Department of Computer Sciences. The CHTC is supported by UW-Madison, the Advanced Computing Initiative, the Wisconsin Alumni Research Foundation, the Wisconsin Institutes for Discovery, and the National Science Foundation, and is an active member of the Open Science Grid, which is supported by the National Science Foundation and the U.S. Department of Energy's Office of Science.

- Arnold, D. W., Xu, C., Kim, E. H. and Neumark, D. M.: Study of low-lying electronic states of ozone by anion photoelectron spectroscopy of O³⁻, *J. Chem. Phys.*, 101(2), 912–922, doi:10.1063/1.467745, 1994.
- Bariteau, L., Helmig, D., Fairall, C. W., Hare, J. E., Hueber, J. and Lang, E. K.: Determination of oceanic ozone deposition by ship-borne eddy covariance flux measurements, *Atmos. Meas. Tech.*, 3(2), 441–455, doi:10.5194/amt-3-441-2010, 2010.
- 690 Barr, A. G., Richardson, A. D., Hollinger, D. Y., Papale, D., Arain, M. A., Black, T. A., Bohrer, G., Dragoni, D., Fischer, M. L., Gu, L., Law, B. E., Margolis, H. A., Mccaughey, J. H., Munger, J. W., Oechel, W. and Schaeffer, K.: Use of change-point detection for friction-velocity threshold evaluation in eddy-covariance studies, *Agric. For. Meteorol.*, 171–172, 31–45, doi:10.1016/j.agrformet.2012.11.023, 2013.
- Bertram, T. H., Kimmel, J. R., Crisp, T. A., Ryder, O. S., Yatavelli, R. L. N., Thornton, J. A., Cubison, M. J., Gonin, M. and
695 Worsnop, D. R.: A field-deployable, chemical ionization time-of-flight mass spectrometer, *Atmos. Meas. Tech.*, 4(7), 1471–1479, doi:10.5194/amt-4-1471-2011, 2011.
- Bey, I., Jacob, D. J., Yantosca, R. M., Logan, J. A., Field, B. D., Fiore, A. M., Li, Q., Liu, H. Y., Mickley, L. J. and Schultz, M. G.: Global modeling of tropospheric chemistry with assimilated meteorology: Model description and evaluation, *J. Geophys. Res. Atmos.*, doi:10.1029/2001JD000807, 2001.
- 700 Blomquist, B. W., Huebert, B. J., Fairall, C. W. and Faloon, I. C.: Determining the sea-air flux of dimethylsulfide by eddy correlation using mass spectrometry, *Atmos. Meas. Tech.*, 3(1), 1–20, doi:10.5194/amt-3-1-2010, 2010.
- Bork, N., Kurtén, T., Enghoff, M. B., Pedersen, J. O. P., Mikkelsen, K. V. and Svensmark, H.: Ab initio studies of O⁻² (H₂O)_n and O⁻³ (H₂O)_n anionic molecular clusters, $n \leq 12$, *Atmos. Chem. Phys.*, 11(14), 7133–7142, doi:10.5194/acp-11-7133-2011, 2011.
- 705 Brophy, P. and Farmer, D. K.: Clustering, methodology, and mechanistic insights into acetate chemical ionization using high-resolution time-of-flight mass spectrometry, *Atmos. Meas. Tech.*, 9(8), 3969–3986, doi:10.5194/amt-9-3969-2016, 2016.
- Chang, W., Heikes, B. G. and Lee, M.: Ozone deposition to the sea surface: Chemical enhancement and wind speed dependence, *Atmos. Environ.*, 38(7), 1053–1059, doi:10.1016/j.atmosenv.2003.10.050, 2004.
- Dorsey, J. R., Duyzer, J. H., Gallagher, M. W., Coe, H., Pilegaard, K., Weststrate, J. H., Jensen, N. O. and Walton, S.: Oxidized
710 nitrogen and ozone interaction with forests. I: Experimental observations and analysis of exchange with Douglas fir, *Q. J. R. Meteorol. Soc.*, doi:10.1256/qj.03.124, 2004.
- Ellis, R. a, Murphy, J. G., Pattey, E., Haarlem, R. Van and Brien, J. M. O.: Characterizing a Quantum Cascade Tunable Infrared Laser Differential Absorption Spectrometer (QC-TILDAS) for measurements of atmospheric ammonia, *Atmos. Meas. Tech.*, (x), 3309–3338, 2010.
- 715 Emmons, L., Lamarque, J., Hess, P. G. and Pfister, G.: Impact of Mexico City on Regional Air Quality from MOZART-4 simulations and MILAGRO observations, *Atmos. Chem. Phys. Discuss.*, 10, 3457–3498, 2010.
- Ervin, K. M., Ho, J. and Lineberger, W. C.: Ultraviolet photoelectron spectrum of nitrite anion, *J. Phys. Chem.*, 92(19), 5405–

- 5412, doi:10.1021/j100330a017, 1988.
- Ervin, K. M., Anusiewicz, I., Skurski, P., Simons, J. and Lineberger, W. C.: The only stable state of O₂⁻ is the X²Π_g ground state and it (still!) has an adiabatic electron detachment energy of 0.45 eV, *J. Phys. Chem. A*, 107(41), 8521–8529, doi:10.1021/jp0357323, 2003.
- Ewing, R. G. and Waltman, M. J.: Production and utilization of CO₃⁻ produced by a corona discharge in air for atmospheric pressure chemical ionization, *Int. J. Mass Spectrom.*, 296(1–3), 53–58, doi:10.1016/j.ijms.2010.08.024, 2010.
- Fairall, C. W., Helmig, D., Ganzeveld, L. and Hare, J.: Water-side turbulence enhancement of ozone deposition to the ocean, *Atmos. Chem. Phys.*, 7(2), 443–451, doi:10.5194/acp-7-443-2007, 2007.
- Fairall, C. W., Yang, M., Bariteau, L., Edson, J. B., Helmig, D., McGillis, W., Pezoa, S., Hare, J. E., Huebert, B. and Blomquist, B.: Implementation of the Coupled Ocean-Atmosphere Response Experiment flux algorithm with CO₂, dimethyl sulfide, and O₃, *J. Geophys. Res. Ocean.*, 116(10), doi:10.1029/2010JC006884, 2011.
- Faloona, I., Lenschow, D. H., Campos, T., Stevens, B., van Zanten, M., Blomquist, B., Thornton, D., Bandy, A. and Gerber, H.: Observations of Entrainment in Eastern Pacific Marine Stratocumulus Using Three Conserved Scalars, *J. Atmos. Sci.*, 62(9), 3268–3285, doi:10.1175/JAS3541.1, 2005.
- Fares, S., McKay, M., Holzinger, R. and Goldstein, A. H.: Ozone fluxes in a *Pinus ponderosa* ecosystem are dominated by non-stomatal processes: Evidence from long-term continuous measurements, *Agric. For. Meteorol.*, 150(3), 420–431, doi:10.1016/j.agrformet.2010.01.007, 2010.
- Finco, A., Coyle, M., Nemitz, E., Marzuoli, R., Chiesa, M., Loubet, B., Fares, S., Diaz-Pines, E., Gasche, R. and Gerosa, G.: Characterization of ozone deposition to a mixed oak-hornbeam forest - Flux measurements at five levels above and inside the canopy and their interactions with nitric oxide, *Atmos. Chem. Phys.*, 18(24), 17945–17961, doi:10.5194/acp-18-17945-2018, 2018.
- Foken, T. and Wichura, B.: Tools for quality assessment of surface-based flux measurements, *Agric. For. Meteorol.*, 78(1–2), 83–105, doi:10.1016/0168-1923(95)02248-1, 1996.
- Fowler, D., Flechard, C., Cape, J. N., Storeton-West, R. L. and Coyle, M.: Measurements of ozone deposition to vegetation quantifying the flux, the stomatal and non-stomatal components, *Water. Air. Soil Pollut.*, doi:10.1023/A:1012243317471, 2001.
- Gallagher, M. W., Beswick, K. M. and Coe, H.: Ozone deposition to coastal waters, *Q. J. R. Meteorol. Soc.*, 127(572), 539–558, doi:10.1256/smsqj.57214, 2001.
- Ganzeveld, L., Helmig, D., Fairall, C. W., Hare, J. and Pozzer, A.: Atmosphere-ocean ozone exchange: A global modeling study of biogeochemical, atmospheric, and waterside turbulence dependencies, *Global Biogeochem. Cycles*, 23(4), 1–16, doi:10.1029/2008GB003301, 2009.
- Güsten, H., Heinrich, G., Schmidt, R. W. H. and Schurath, U.: A novel ozone sensor for direct eddy flux measurements, *J. Atmos. Chem.*, 14(1–4), 73–84, doi:10.1007/BF00115224, 1992.
- Helmig, D., Ganzeveld, L., Butler, T. and Oltmans, S. J.: The role of ozone atmosphere-snow gas exchange on polar, boundary-

- layer tropospheric ozone - A review and sensitivity analysis, *Atmos. Chem. Phys.*, 7(1), 15–30, doi:10.5194/acp-7-15-2007, 2007.
- Helmig, D., Lang, E. K., Bariteau, L., Boylan, P., Fairall, C. W., Ganzeveld, L., Hare, J., Huebert, B. J. and Pallandt, M.: Atmosphere-ocean ozone fluxes during the TexAQS 2006, STRATUS 2006, GOMECC 2007, GasEx 2008, and AMMA 2008 cruises, *J. Geophys. Res. Atmos.*, 117(D4), doi:10.1029/2011JD015955, 2012.
- Horst, T. W.: A simple formula for attenuation of eddy fluxes measured with first-order-response scalar sensors, *Boundary-Layer Meteorol.*, 82(2), 219–233, doi:10.1023/A:1000229130034, 1997.
- Huey, L. G.: The kinetics of the reaction of Cl-, O-, and O2- with HNO3: implications for measurements of HNO3 in the atmosphere, *Int. J. Mass Spectrom.*, 153, 145–150, 1996.
- Hunton, D. E., Hofmann, M., Lindeman, T. G. and Castleman, A. W.: Photodissociation dynamics of CO3-, , 82(1), 134–150, 1985.
- Ikawa, H. and Oechel, W. C.: Temporal variations in air-sea CO2 exchange near large kelp beds near San Diego, California, *J. Geophys. Res. Ocean.*, 120(1), 50–63, doi:10.1002/2014JC010229, 2015.
- Kaimal, J. C., Wyngaard, J. C., Izumi, Y. and Coté, O. R.: Spectral characteristics of surface-layer turbulence, *Q. J. R. Meteorol. Soc.*, 98(417), 563–589, doi:10.1002/qj.49709841707, 1972.
- Kawa, S. R. and Pearson, R.: Ozone budgets from the dynamics and chemistry of marine stratocumulus experiment, *J. Geophys. Res.*, 94(D7), 9809–9817, doi:10.1029/JD094iD07p09809, 1989.
- Keronen, P., Reissell, A., Rannik, Ü., Pohja, T., Siivola, E., Hiltunen, V., Hari, P., Kulmala, M. and Vesala, T.: Ozone flux measurements over a Scots pine forest using eddy covariance method: Performance evaluation and comparison with flux-profile method, *Boreal Environ. Res.*, 8(4), 425–443, 2003.
- Kim, M. J., Farmer, D. K. and Bertram, T. H.: A controlling role for the air-sea interface in the chemical processing of reactive nitrogen in the coastal marine boundary layer, *Proc Natl Acad Sci U S A*, 111(11), 3943–3948, doi:10.1073/pnas.1318694111, 2014.
- Kim, M. J., Novak, G. A., Zoerb, M. C., Yang, M., Blomquist, B. W., Huebert, B. J., Cappa, C. D. and Bertram, T. H.: Air-Sea exchange of biogenic volatile organic compounds and the impact on aerosol particle size distributions, *Geophys. Res. Lett.*, 44(8), 3887–3896, doi:10.1002/2017GL072975, 2017.
- Kleindienst, T. E., Hudgens, E. E., Smith, D. F., McElroy, F. F. and Bufalini, J. J.: Comparison of chemiluminescence and ultraviolet ozone monitor responses in the presence of humidity and photochemical pollutants, *Air Waste*, 43(2), 213–222, doi:10.1080/1073161X.1993.10467128, 1993.
- Kurpius, M. R. and Goldstein, A. H.: Gas-phase chemistry dominates O3 loss to a forest, implying a source of aerosols and hydroxyl radicals to the atmosphere, *Geophys. Res. Lett.*, doi:10.1029/2002GL016785, 2003.
- Kurtenbach, R., Vaupel, K., Kleffmann, J., Klenk, U., Schmidt, E. and Wiesen, P.: Emissions of NO, NO2 and PM from inland shipping, *Atmos. Chem. Phys.*, 16(22), 14285–14295, doi:10.5194/acp-16-14285-2016, 2016.
- Lamarque, J. F., Emmons, L. K., Hess, P. G., Kinnison, D. E., Tilmes, S., Vitt, F., Heald, C. L., Holland, E. A., Lauritzen, P.

- H., Neu, J., Orlando, J. J., Rasch, P. J. and Tyndall, G. K.: CAM-chem: Description and evaluation of interactive atmospheric chemistry in the Community Earth System Model, *Geosci. Model Dev.*, 5(2), 369–411, doi:10.5194/gmd-5-369-2012, 2012.
- Langford, B., Acton, W., Ammann, C., Valach, A. and Nemitz, E.: Eddy-covariance data with low signal-to-noise ratio: Time-lag determination, uncertainties and limit of detection, *Atmos. Meas. Tech.*, 8(10), 4197–4213, doi:10.5194/amt-8-4197-2015, 790 2015.
- Lenschow, D. H. and Kristensen, L.: Uncorrelated Noise in Turbulence Measurements, *J. Atmos. Ocean. Technol.*, 2, 68–81, doi:https://doi.org/10.1175/1520-0426(1985)002<0068:UNITM>2.0.CO;2, 1985.
- Lenschow, D. H., Pearson, R. and Stankov, B. B.: Estimating the ozone budget in the boundary layer by use of aircraft measurements of ozone eddy flux and mean concentration, *J. Geophys. Res.*, 86(C8), 7291, doi:10.1029/JC086iC08p07291, 795 1981.
- Lenschow, D. H., Pearson, R. J. and Stankov, B. B.: Measurements of Ozone Vertical Flux to Ocean and Forest, *J. Geophys. Res.*, 87(C11), 8833–8837, doi:10.1029/JC087iC11p08833, 1982.
- Liu, W. T., Tang, W. and Niler, P. P.: Humidity Profiles over the Ocean, *J. Clim.*, 4(10), 1023–1034, 1991.
- Luhar, A. K., Galbally, I. E., Woodhouse, M. T. and Thatcher, M.: An improved parameterisation of ozone dry deposition to the ocean and its impact in a global climate-chemistry model, *Atmos. Chem. Phys.*, 17(5), 3749–3767, doi:10.5194/acp-17-3749-2017, 2017. 800
- Massman, W. J.: The attenuation of concentration fluctuations in turbulent flow through a tube, *J. Geophys. Res. Atmos.*, 96(D8), 15269–15273, doi:10.1029/91JD01514, 1991.
- McKay, W. A., Stephens, B. A. and Dollard, G. J.: Laboratory measurements of ozone deposition to sea water and other saline solutions, *Atmos. Environ. Part A, Gen. Top.*, doi:10.1016/0960-1686(92)90467-Y, 1992. 805
- Muller, J. B. A., Percival, C. J., Gallagher, M. W., Fowler, D., Coyle, M. and Nemitz, E.: Sources of uncertainty in eddy covariance ozone flux measurements made by dry chemiluminescence fast response analysers, *Atmos. Meas. Tech.*, 3(1), 163–176, doi:10.5194/amt-3-163-2010, 2010.
- Nguyen, T. B., Crounse, J. D., Teng, A. P., St. Clair, J. M., Paulot, F., Wolfe, G. M. and Wennberg, P. O.: Rapid deposition of oxidized biogenic compounds to a temperate forest, *Proc. Natl. Acad. Sci.*, 112(5), E392–E401, doi:10.1073/pnas.1418702112, 2015. 810
- O’Sullivan, D. W., Silwal, I. K. C., McNeill, A. S., Treadaway, V. and Heikes, B. G.: Quantification of gas phase hydrogen peroxide and methyl peroxide in ambient air: Using atmospheric pressure chemical ionization mass spectrometry with O₂⁻, and O₂⁻(CO₂) reagent ions, *Int. J. Mass Spectrom.*, doi:10.1016/j.ijms.2017.11.015, 2018.
- Papale, D., Reichstein, M., Aubinet, M., Canfora, E., Bernhofer, C., Kutsch, W., Longdoz, B., Rambal, S., Valentini, R., Vesala, T. and Yakir, D.: Towards a standardized processing of Net Ecosystem Exchange measured with eddy covariance technique: Algorithms and uncertainty estimation, *Biogeosciences*, 3(4), 571–583, doi:10.5194/bg-3-571-2006, 2006. 815
- Pearson, R.: Measuring ambient ozone with high sensitivity and bandwidth, *Rev. Sci. Instrum.*, 61(2), 907–916, doi:10.1063/1.1141462, 1990.

- 820 Porter, J. G., De Bruyn, W. and Saltzman, E. S.: Eddy flux measurements of sulfur dioxide deposition to the sea surface, *Atmos. Chem. Phys.*, 18(20), 15291–15305, doi:10.5194/acp-18-15291-2018, 2018.
- Reiner, T., Möhler, O. and Arnold, F.: Improved atmospheric trace gas measurements with an aircraft-based tandem mass spectrometer: Ion identification by mass-selected fragmentation studies, *J. Geophys. Res. Atmos.*, 103(D23), 31309–31320, doi:10.1029/1998JD100003, 1998.
- 825 Rienstra-Kiracofe, J. C., Tschumper, G. S., Schaefer, H. F., Nandi, S. and Ellison, G. B.: Atomic and molecular electron affinities: Photoelectron experiments and theoretical computations, *Chem. Rev.*, 102(1), 231–282, doi:10.1021/cr990044u, 2002.
- Snodgrass, J. T., Roehl, C. M., Van Koppen, P. A. M., Palke, W. E. and Bowers, M. T.: Photodissociation of CO₃⁻: Product kinetic energy measurements as a probe of excited state potential surfaces and dissociation dynamics, *J. Chem. Phys.*, 92(10), 830 5935–5943, doi:10.1063/1.458363, 1990.
- Spirig, C., Neftel, A., Ammann, C., Dommen, J., Grabmer, W., Thielmann, A., Schaub, A., Beauchamp, J., Wisthaler, A. and Hansel, A.: Eddy covariance flux measurements of biogenic VOCs during ECHO 2003 using proton transfer reaction mass spectrometry, *Atmos. Chem. Phys.*, 5, 465–481, doi:10.5194/acp-5-465-2005, 2005.
- Stella, P., Kortner, M., Ammann, C., Foken, T., Meixner, F. X. and Trebs, I.: Measurements of nitrogen oxides and ozone 835 fluxes by eddy covariance at a meadow: Evidence for an internal leaf resistance to NO₂, *Biogeosciences*, doi:10.5194/bg-10-5997-2013, 2013.
- Taipale, R., Ruuskanen, T. M. and Rinne, J.: Lag time determination in DEC measurements with PTR-MS, *Atmos. Meas. Tech.*, doi:10.5194/amt-3-853-2010, 2010.
- Thornton, D. C., Bandy, A. R., Tu, F. H., Blomquist, B. W., Mitchell, G. M., Nadler, W. and Lenschow, D. H.: Fast airborne 840 sulfur dioxide measurements by Atmospheric Pressure Ionization Mass Spectrometry (APIMS), *J. Geophys. Res. Atmos.*, doi:10.1029/2002JD002289, 2002a.
- Thornton, J. A., Wooldridge, P. J. and Cohen, R. C.: Atmospheric NO₂: In Situ Laser-Induced Fluorescence Detection at Parts per Trillion Mixing Ratios, *Anal. Chem.*, 72(3), 528–539, doi:10.1021/ac9908905, 2002b.
- Tuovinen, J. P., Ashmore, M. R., Emberson, L. D. and Simpson, D.: Testing and improving the EMEP ozone deposition 845 module, in *Atmospheric Environment*, 2004.
- Veres, P., Roberts, J. M., Warneke, C., Welsh-Bon, D., Zahniser, M., Herndon, S., Fall, R. and de Gouw, J.: Development of negative-ion proton-transfer chemical-ionization mass spectrometry (NI-PT-CIMS) for the measurement of gas-phase organic acids in the atmosphere, *Int. J. Mass Spectrom.*, 274(1–3), 48–55, doi:10.1016/j.ijms.2008.04.032, 2008.
- Vermeuel, M. P., Novak, G. A., Alwe, H. D., Hughes, D. D., Kaleel, R., Dickens, A. F., Kenski, D., Czarnetzki, A. C., Stone, 850 E. A., Stanier, C. O., Pierce, R. B., Millet, D. B. and Bertram, T. H.: Sensitivity of Ozone Production to NO_x and VOC Along the Lake Michigan Coastline, *J. Geophys. Res. Atmos.*, 124(20), 10989–11006, doi:10.1029/2019JD030842, 2019.
- Voisin, D., Smith, J. N., Sakurai, H., McMurry, P. H. and Eisele, F. L.: Thermal desorption chemical ionization mass spectrometer for ultrafine particle chemical composition, *Aerosol Sci. Technol.*, 37(6), 471–475,

doi:10.1080/02786820300959, 2003.

- 855 Webb, E. K., Pearman, G. I. and Leuning, R.: Correction of flux measurements for density effects due to heat and water vapour transfer, *Q. J. Roy. Meteorol. Soc.*, 106(447), 85–100, doi:http://dx.doi.org/10.1002/qj.49710644707, 1980.
- Weinheimer, A. J.: *Chemical Methods: Chemiluminescence, Chemical Amplification, Electrochemistry, and Derivation*, in *Analytical Techniques for Atmospheric Measurement.*, 2007.
- Werle, P., Mücke, R. and Slemr, F.: The Limits of Signal Averaging in Atmospheric Trace-Gas Monitoring by Tunable Diode-
860 Laser Absorption Spectroscopy (TDLAS), , 139, 131–139, 1993.
- Wesely, M. L. and Hicks, B. B.: A review of the current status of knowledge on dry deposition, *Atmos. Environ.*, doi:10.1016/S1352-2310(99)00467-7, 2000.
- Wesely, M. L., Cook, D. R. and Williams, R. M.: Field measurement of small ozone fluxes to snow, wet bare soil, and lake water, *Boundary-Layer Meteorol.*, 20(4), 459–471, doi:10.1007/BF00122295, 1981.
- 865 Wienhold, F. G., Welling, M. and Harris, G. W.: Micrometeorological measurement and source region analysis of nitrous oxide fluxes from an agricultural soil, *Atmos. Environ.*, 29(17), 2219–2227, doi:10.1016/1352-2310(95)00165-U, 1995.
- Wilczak, J. M., Oncley, S. P. and Stage, S. A.: Sonic anemometer tilt correction algorithms, *Boundary-Layer Meteorol.*, 99(1), 127–150, doi:10.1023/a:1018966204465, 2001.
- Wolfe, G. M., Hanisco, T. F., Arkinson, H. L., Bui, T. P., Crouse, J. D., Dean-Day, J., Goldstein, A., Guenther, A., Hall, S.
870 R., Huey, G., Jacob, D. J., Karl, T., Kim, P. S., Liu, X., Marvin, M. R., Mikoviny, T., Misztal, P. K., Nguyen, T. B., Peischl, J., Pollack, I., Ryerson, T., St. Clair, J. M., Teng, A., Travis, K. R., Ullmann, K., Wennberg, P. O. and Wisthaler, A.: Quantifying sources and sinks of reactive gases in the lower atmosphere using airborne flux observations, *Geophys. Res. Lett.*, 42(19), 8231–8240, doi:10.1002/2015gl065839, 2015.
- Yang, M., Beale, R., Smyth, T. and Blomquist, B.: Measurements of OVOC fluxes by eddy covariance using a proton-transfer-
875 reaction mass spectrometer-method development at a coastal site, *Atmos. Chem. Phys.*, 13(13), 6165–6184, doi:10.5194/acp-13-6165-2013, 2013.
- Yang, M., Prytherch, J., Kozlova, E., Yelland, M. J., Parenkat Mony, D. and Bell, T. G.: Comparison of two closed-path cavity-based spectrometers for measuring air-water CO₂ and CH₄ fluxes by eddy covariance, *Atmos. Meas. Tech.*, 9(11), 5509–5522, doi:10.5194/amt-9-5509-2016, 2016.
- 880 Yienger, J. J. and Levy, H.: Empirical model of global soil-biogenic NO_x emissions , *J. Geophys. Res.*, doi:10.1029/95jd00370, 2004.
- Zafiriou, O. C. and McFarland, M.: Nitric oxide from nitrite photolysis in the central equatorial Pacific., *J. Geophys. Res.*, 86(C4), 3173–3182, doi:10.1029/JC086iC04p03173, 1981.
- Zahn, A., Weppner, J., Widmann, H., Schlote-Holubek, K., Burger, B., Kühner, T. and Franke, H.: A fast and precise
885 chemiluminescence ozone detector for eddy flux and airborne application, *Atmos. Meas. Tech.*, 5(2), 363–375, doi:10.5194/amt-5-363-2012, 2012.
- Zhang, L., Brook, J. R. and Vet, R.: A revised parameterization for gaseous dry deposition in air-quality models, *Atmos. Chem.*

890

895

900

905

| 910

915

Species	Normalized Sensitivity (8 g kg ⁻¹ SH, 1σ)	Absolute Sensitivity (8 g kg ⁻¹ SH)	LOD optimum	LOD (1 Hz)	LOD (10 Hz)	Background (cps, 1σ)	Precision (10 Hz)	Field Calibration R ²
O ₃	12.4 ± 1.2 ncps pptv ⁻¹	180 cps pptv ⁻¹	4.0 pptv (11s)	13 pptv	42 pptv	3.1 × 10 ⁵ ± 5.0 × 10 ⁴	0.74%	0.99
NO ₂	6.7 ± 1.0 ncps pptv ⁻¹	97 cps pptv ⁻¹	2.3 pptv (19s)	9.9 pptv	32 pptv	5.1 × 10 ⁴ ± 1 × 10 ⁴	1.1%	— — —

Table 1. Summary of instrument sensitivity, precision, and accuracy for detection of O₃ and NO₂ from laboratory calibrations. Sensitivity is reported at a specific humidity (SH) of 8 g kg⁻¹ which corresponds to 40% RH at 25 °C. All limits of detection (LOD) are for a S/N = 3. The optimum LOD is reported as the LOD at the optimum averaging time determined by the minimum of the Allan variance spectrum. Optimum averaging times were determined to be 11 s for O₃ and 19 s for NO₂. The reported field comparison (R²) is from a regression of 1-minute bin averaged ozone concentration from the Ox-CIMS with an EPA (Thermo-Fisher 49i) monitor in Zion, IL during four weeks of ambient observation shown in Fig. 7.

920

925

930

935

940

Species	Concentration Mean (ppb) & 1 σ range	5 th to 95 th percentile Concentration Range (ppbv)	v_d mean (cm s ⁻¹)	v_d 20-80% range (cm s ⁻¹)	v_d LOD 1.96 σ (cm s ⁻¹)
O ₃	38.9 ± 12.3	16.9 – 56.9	0.011	-0.0048 – 0.0249	0.0042
NO ₂	4.7 ± 5.5	0.45-16.9	-----	-----	-----

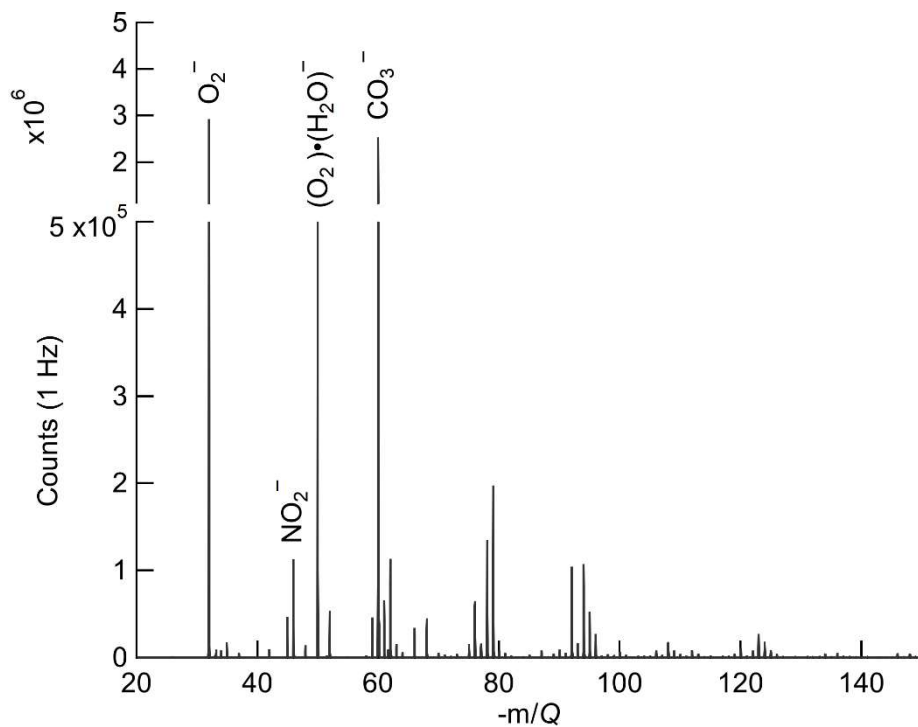
Species	Concentration Mean (ppb) & 1 σ range	5 th to 95 th percentile Concentration Range (ppbv)	v_d mean (cm s ⁻¹)	v_d 20-80% range (cm s ⁻¹)	v_d LOD 1.96 σ (cm s ⁻¹)
O ₃	41.2± 10.1	28.9 – 67.1	0.013	-0.0011 – 0.027	0.0027
NO ₂	4.7 ± 5.5	0.45-16.9	-----	-----	-----

945

Table 2. Overview of flux and concentration measurements of O₃ and NO₂ from Scripps Pier. Concentration ranges are reported for all periods of onshore winds. Flux results are reported only for final quality-controlled flux periods. Ozone mean deposition velocity (v_d) was well resolved from the campaign ensemble average LOD of 0.0042 cm s⁻¹. Reported v_d LOD is the ensemble mean of the LOD determined by the RMSE method at long lag times for each 27-minute flux period. 39% of quality-controlled flux periods fell below the campaign ensemble LOD. Deposition velocity of NO₂ across the air-sea interface is expected to be small (<0.002 cm s⁻¹) and was consistently below the LOD of our instrument so no values are reported here.

950

955



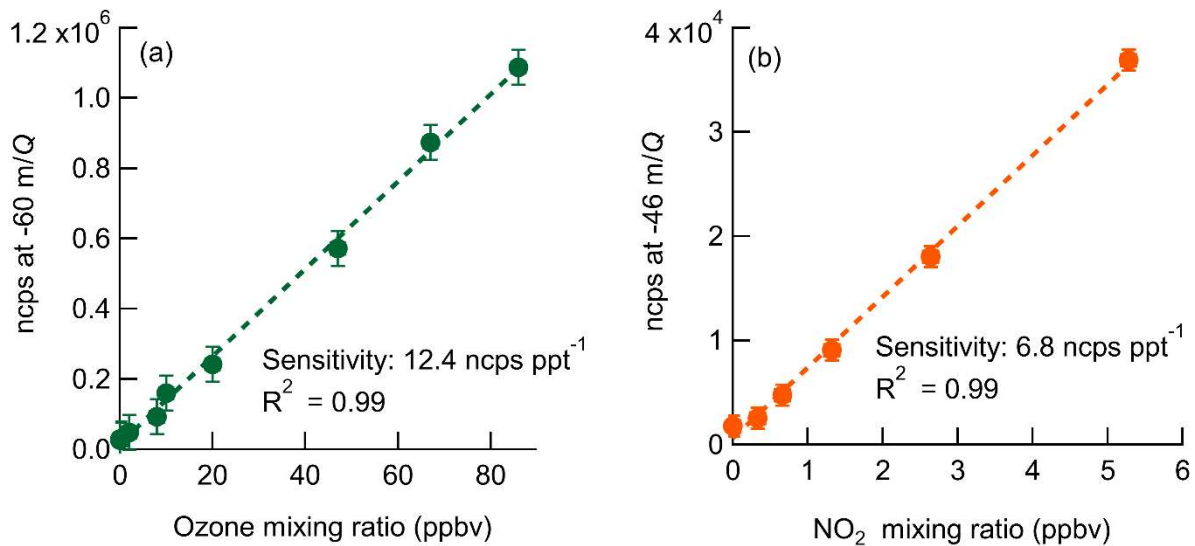
960

Figure 1: Ox-CIMS mass spectra collected at 1 Hz and mass resolution of 950 $M/\Delta M$ (at -60 m/Q), with major peaks highlighted. O_2^- and $O_2(H_2O)^-$ at -32 m/Q and -50 m/Q respectively are the two observed forms of the reagent ion. The detected ozone product (CO_3^- , -60 m/Q) is of comparable magnitude to the O_2^- reagent ion during ambient sampling. NO_2 is detected as the charge transfer product NO_2^- at -46 m/Q. Masses greater than -150 m/Q contribute less than 2% to the total signal and are not plotted.

965

970

975



980 **Figure 2: Normalized calibration curves of O₃ (a) and NO₂ (right) at 8 g kg⁻¹ specific humidity (approximately 40% RH at 25 °C). Ozone is detected as CO₃⁻ at -60 m/Q. NO₂ is detected as the charge transfer product (NO₂⁻) at -46 m/Q. Error bars are the standard deviation in normalized count rate for each measurement point.**

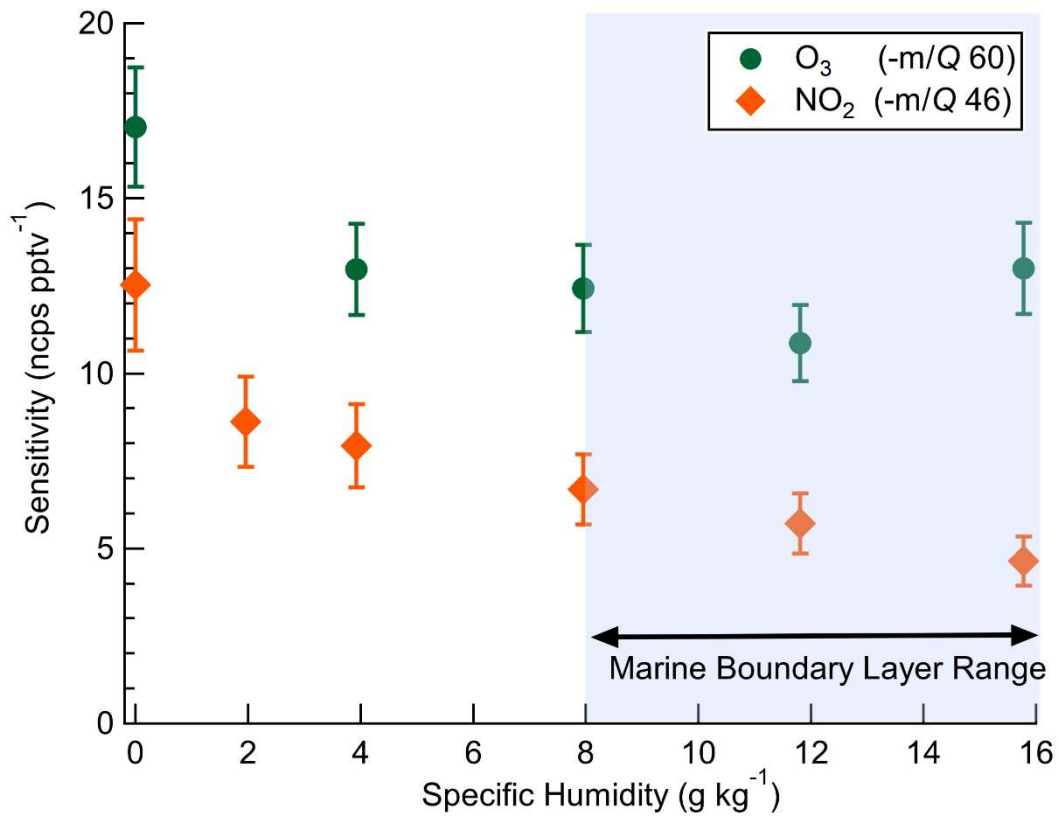


Figure 3: Dependence of O₃ and NO₂ sensitivities on specific humidity. Error bars indicate standard deviation of triplicate calibration curves. The blue shaded region from SH 8–16 g kg⁻¹ is the approximate typical range of specific humidity in the mid-latitude marine boundary layer.

985

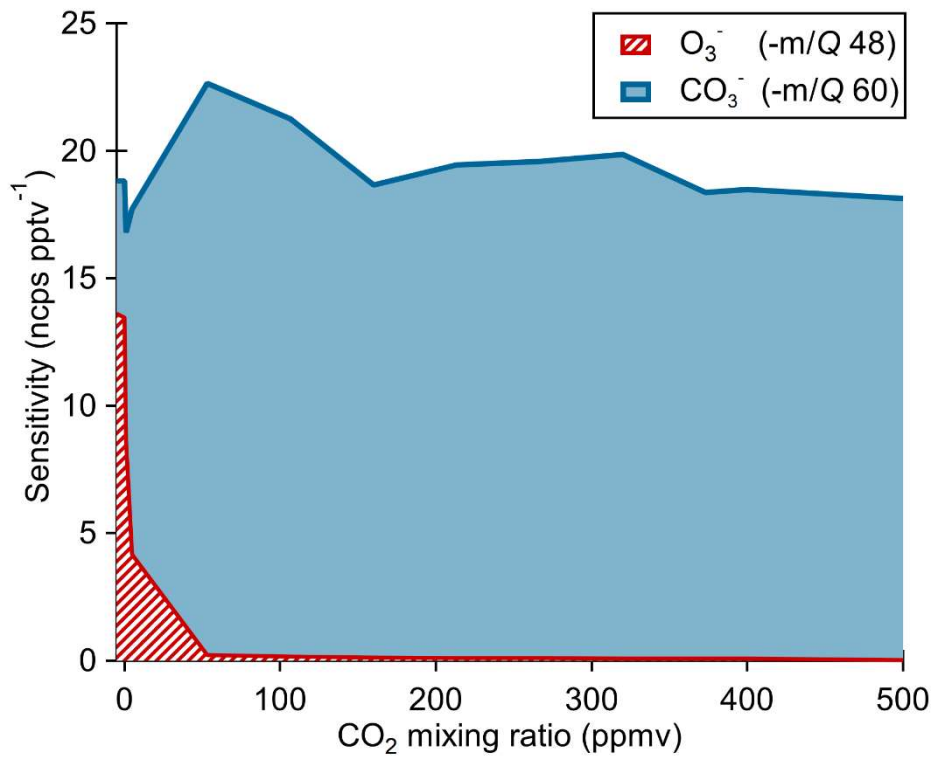


Figure 4: Ox-CIMS cumulative sensitivity to O₃ detected either directly as O₃⁻ or as CO₃⁻ as a function of CO₂ mixing ratio. The sum of sensitivity as O₃⁻ and CO₃⁻ shows that total sensitivity to O₃ is conserved as the product distribution shifts with CO₂ mixing ratio. Greater than 99% of O₃ is observed as CO₃⁻ at CO₂ mixing ratios greater than 60 ppmv.

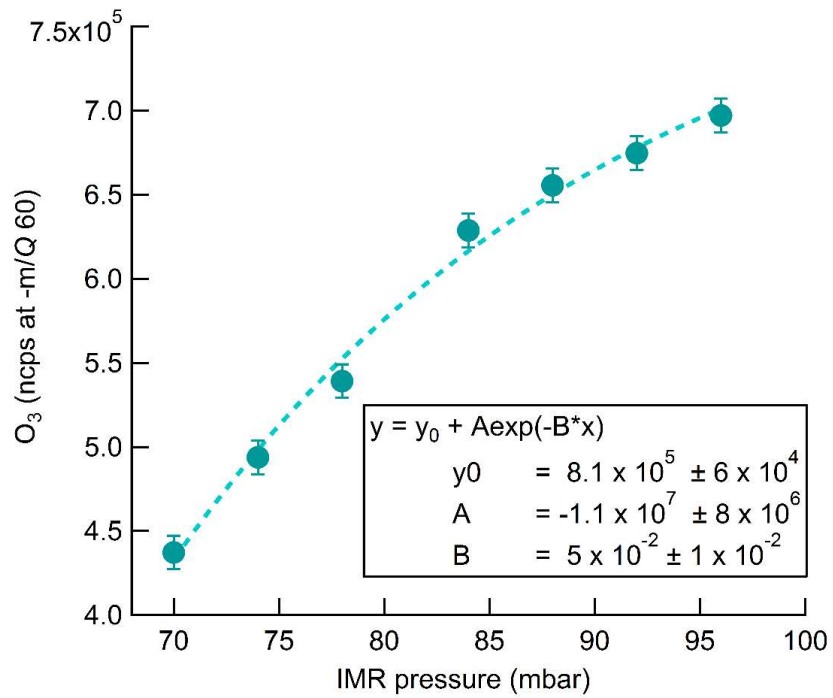
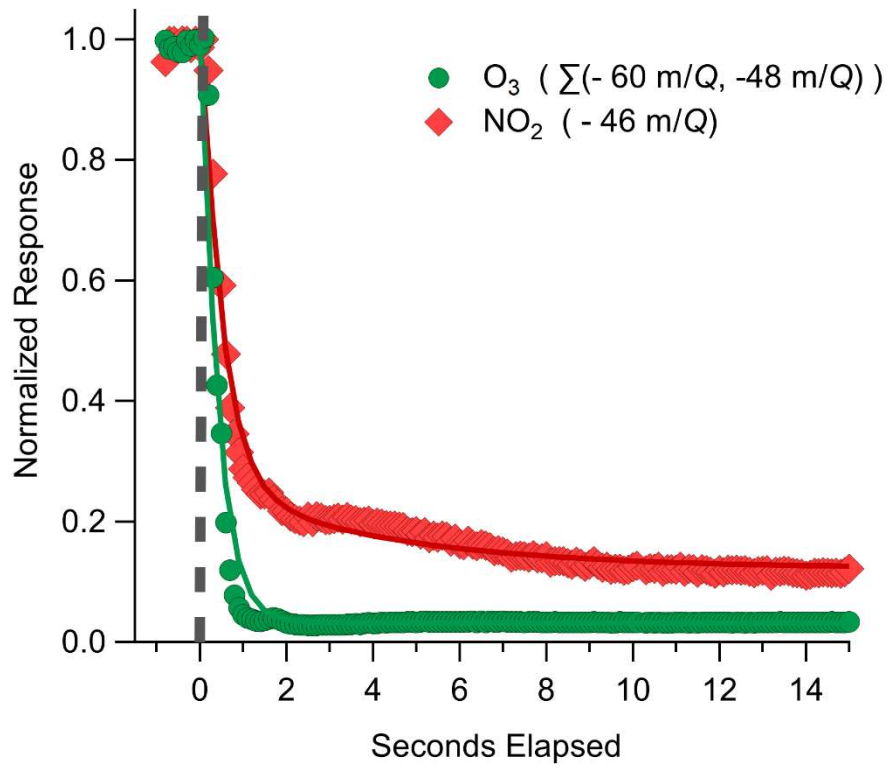


Figure 5. Normalized count rate of CO_3^- (-60 m/Q) ozone detection product as a function of pressure in the IMR during sampling of a constant 35 ppbv O_3 source. The exponential fit of the data is shown by the dashed line. Fit parameters are included to allow for calculation of potential sensitivity improvements with further increase in IMR pressure.



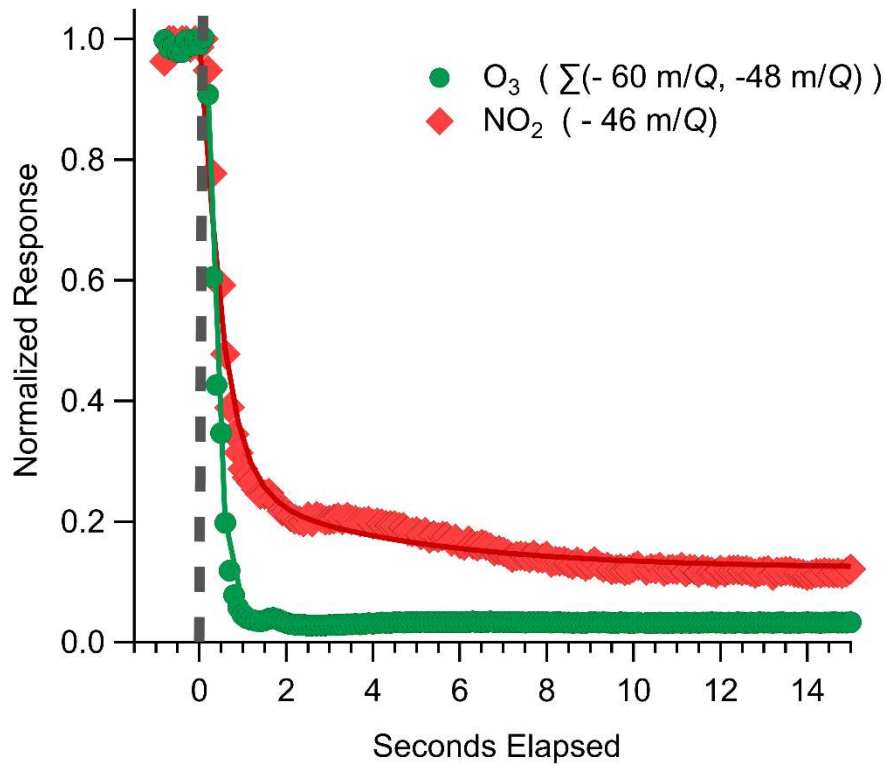
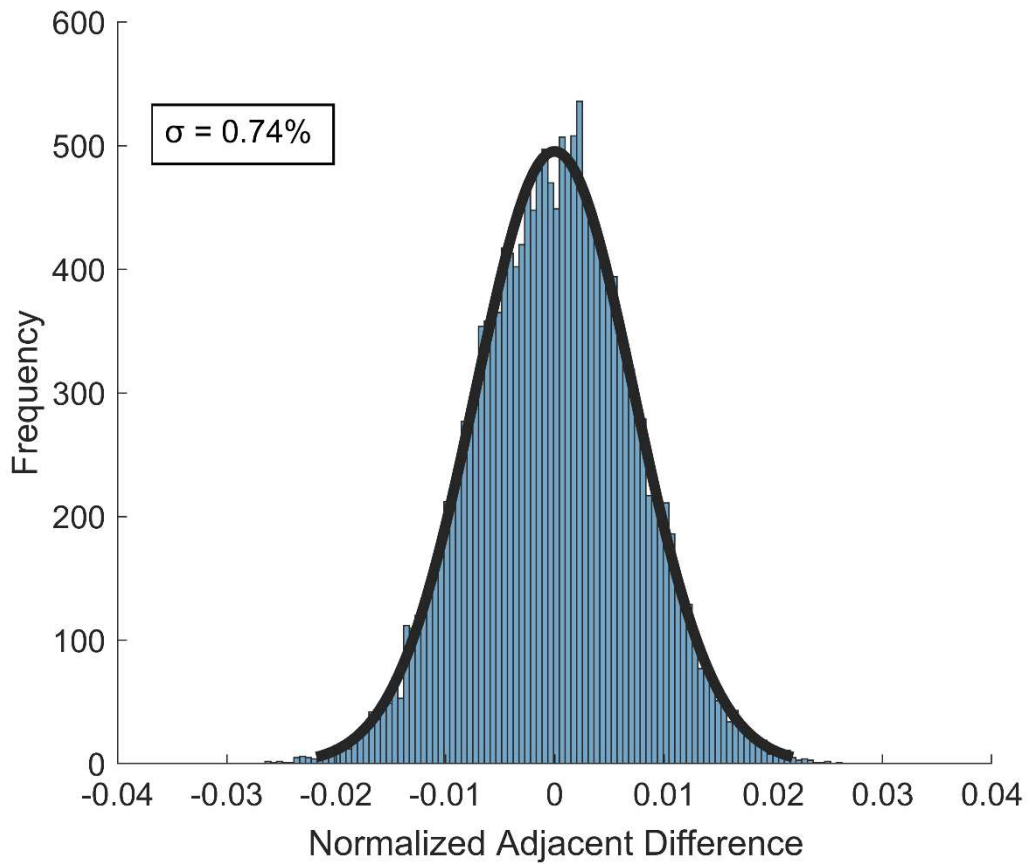


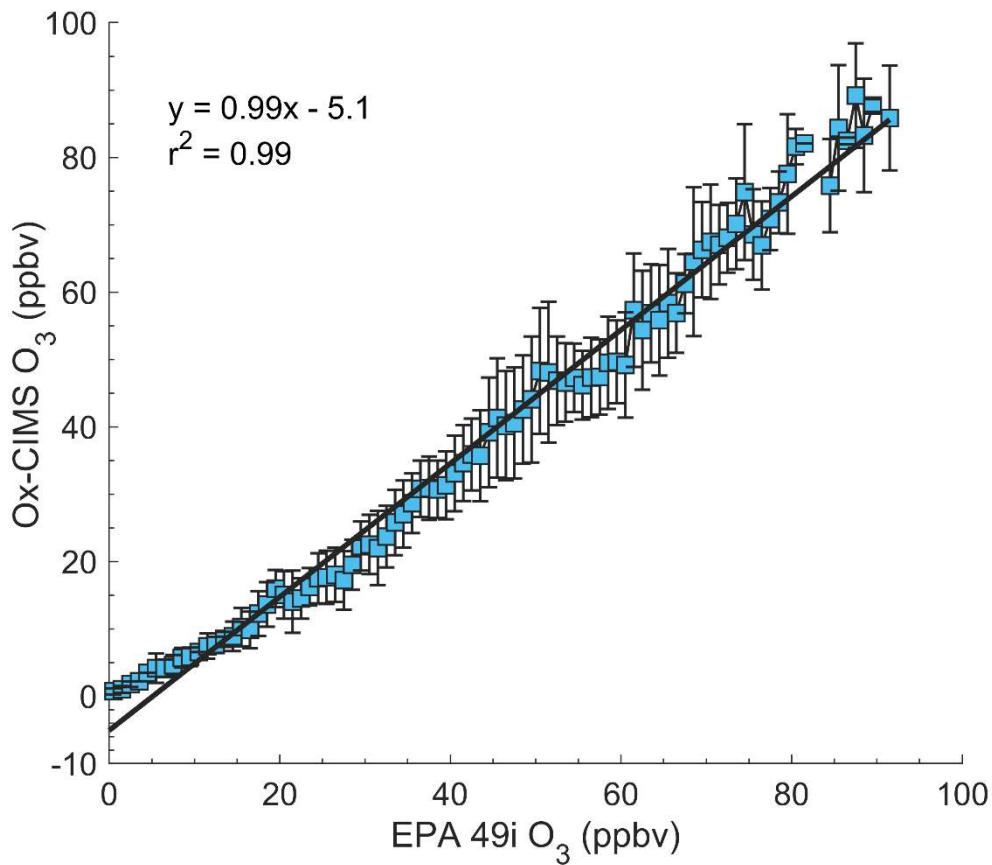
Figure 6: Representative instrument backgrounding determination for O₃ and NO₂ where the inlet was rapidly switched from ambient sampling to an overflow with dry UHP N₂ indicated by the grey dashed line. O₃ response is fit to a bi-exponential decay, plotted as solid lines with a mean response time of 0.28 s. NO₂ is fit to a bi-exponential decay where the initial rapid decay (τ_1) is attributed to gas evacuation of the inlet line and the second slower decay (τ_2) is attributed to equilibration with the inlet walls. Best fit estimates for τ_1 of O₃ and NO₂ were from 0.7 to 1.2 seconds. τ_2 for O₃ was negligible at 0.3 s indicating O₃ has minimal interactions with the walls. τ_2 for NO₂ was determined to be 3.2 s for this decay period.

1000

1005



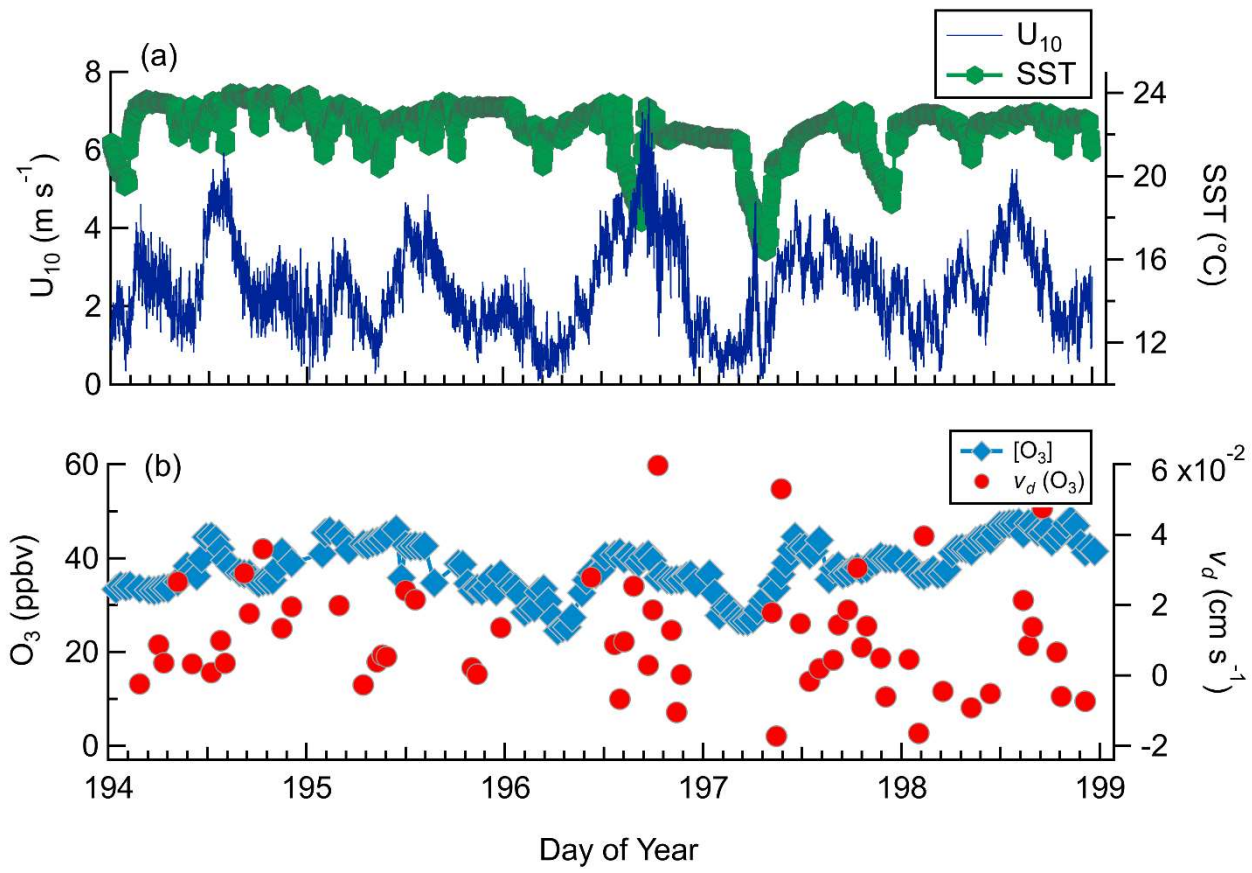
1010 **Figure 7: Distribution of normalized adjacent differences measured at 10 Hz during a stable 27-minute ambient sampling period of 38 ppbv O₃ from Scripps Pier. The 1 σ value of the distribution gives an upper limit of instrument precision of 0.74%.**



1015

Figure 8: Regression of 1-minute average O₃ mixing ratios from the Ox-CIMS against an EPA O₃ monitor (Thermo-Fisher 49i) binned to 1 ppbv over four weeks of ambient sampling in Zion, Illinois in May- June 2017. The solid black line is the linear least-squares regression. Error bars represent the standard deviation of each bin. Instrument agreement is strong for O₃ greater than 10 ppbv, with an apparent bias in one or both instruments below 10 ppbv.

1020



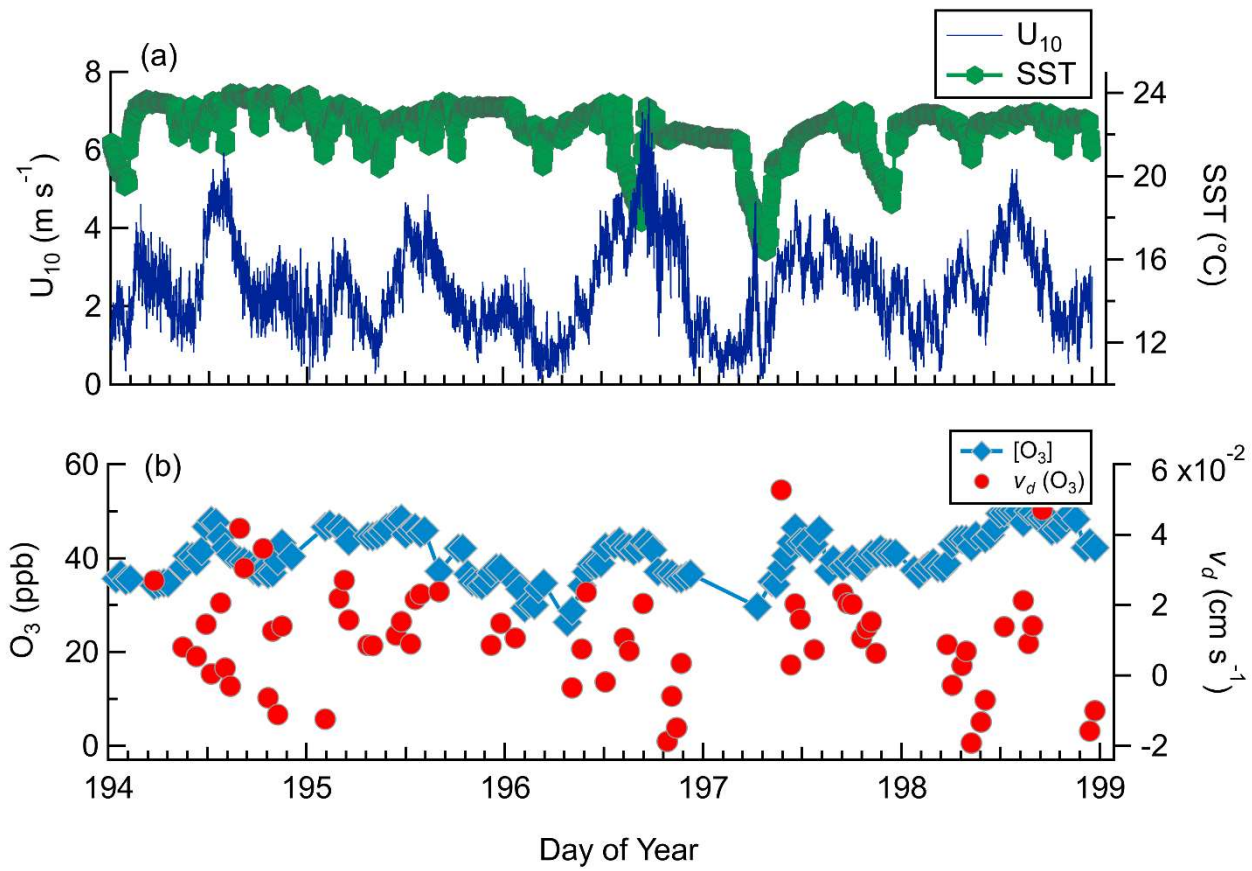


Figure 9: Observed meteorology and O_3 mixing ratio and deposition velocities for DOY 194-199 from Scripps Pier (a) Horizontal wind speed (U_{10}) and sea-surface temperature (SST). (b) O_3 mixing ratios and $v_d(\text{O}_3)$.

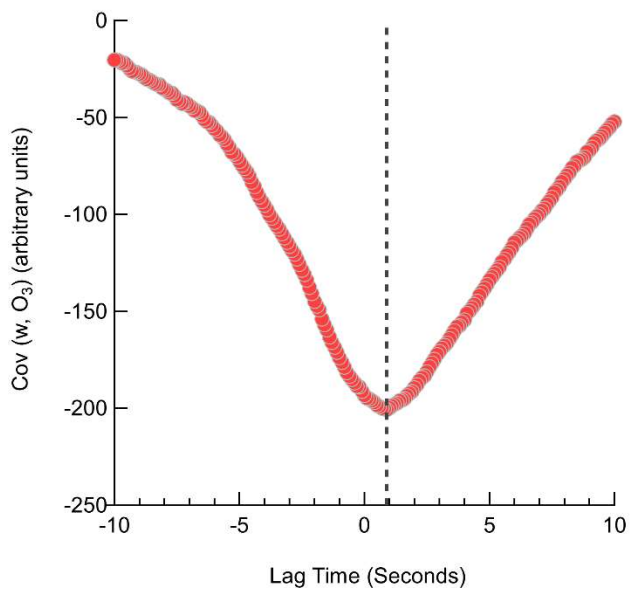
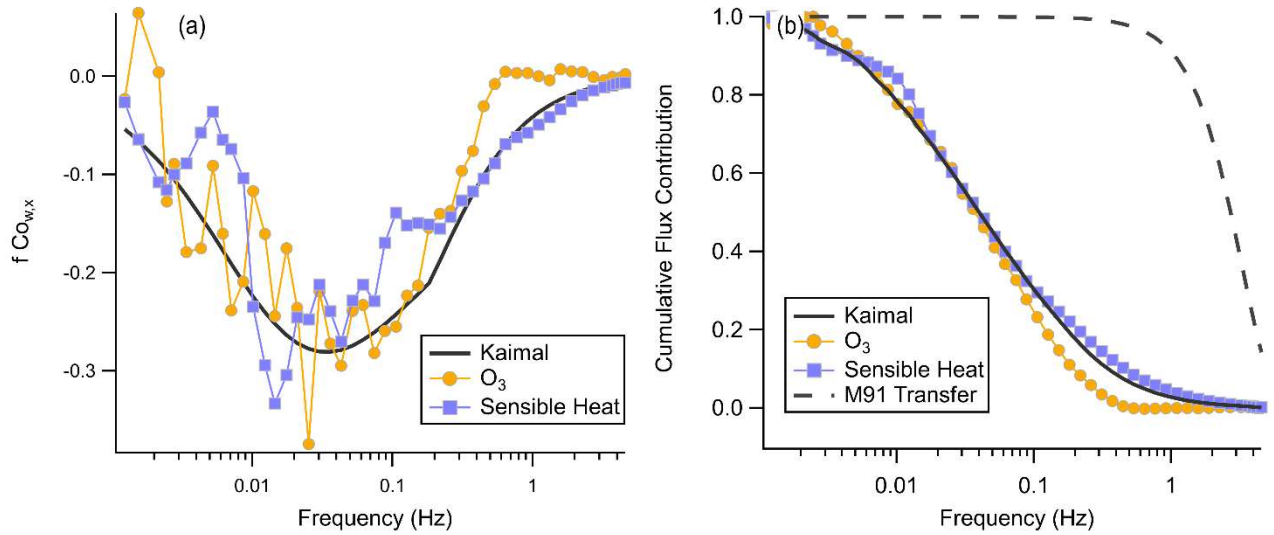


Figure 10: Lag time determination for an individual 27-minute O₃ flux averaging period. The lag time for this flux period determined from the maximum of the covariance to be 0.9 seconds which compares reasonably with the volumetric evacuation time of the inlet of 1.7 to 2.1 seconds.

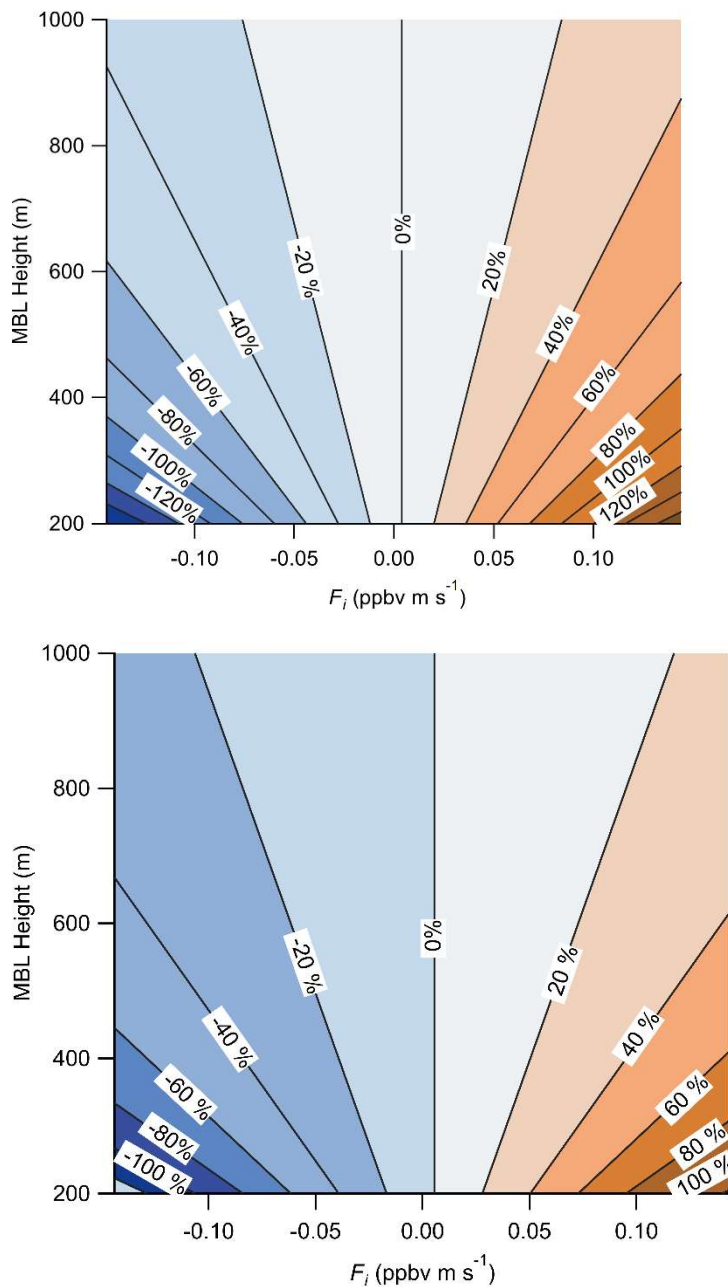
1030

1035



1040 **Figure 11. (a) Mean binned frequency weighted cospectra O_3 and sensible heat flux with vertical wind from the average of two consecutive flux periods from 14:10 – 15:20 local time on July 20th. The Kaimal trace is the idealized cospectra Kaimal et al. (1972) for mean windspeed of 4.4 m s^{-1} and an unstable atmosphere. The sensible heat trace is inverted, and the observed net sensible heat flux was positive for this period (b) Corresponding ogives for cospectra shown in (a). The M91 Transfer trace is the calculated transfer function for turbulent attenuation in a tube from (Massman, 1991).**

1045



1050 **Figure 12. Calculated percent error in the measured O₃ surface flux due to entrainment from the free troposphere as a function of the MBL height and the entrainment flux (F_i). Entrainment flux is the product of the free troposphere to boundary layer concentration gradient (ΔC), and the entrainment velocity (w_e). Calculation of percent error used the Scripps Pier measuring height of 13 m, and mean surface flux of -54.64×10^{-3} ppbv m s⁻¹.**

1055

1060

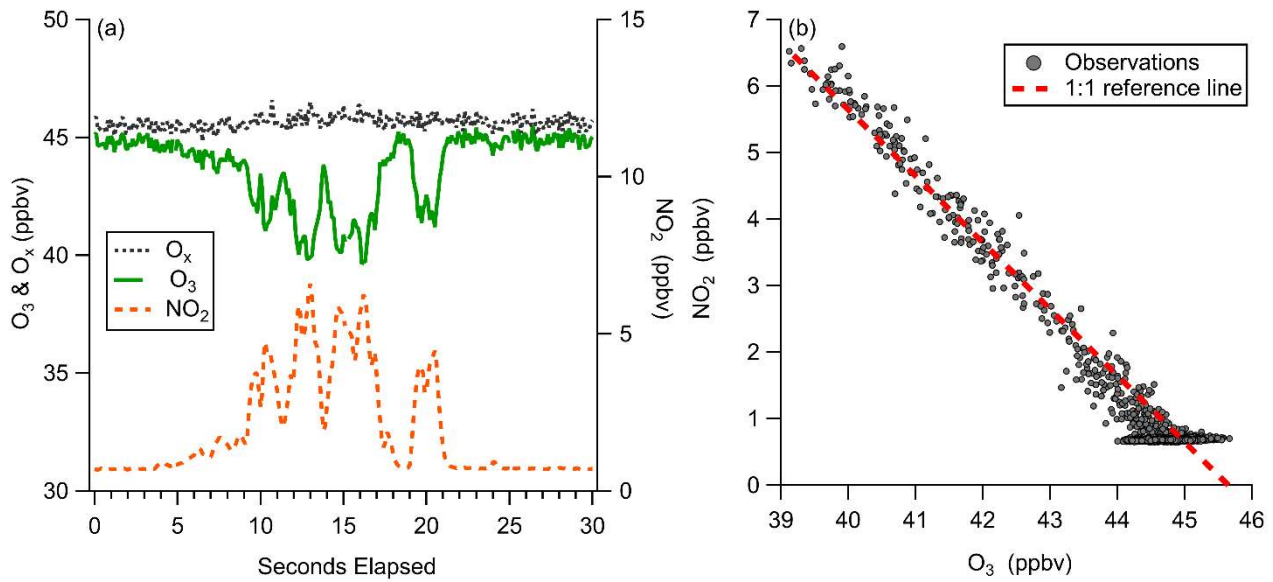


Figure 13: Observations of ozone titration by NO emissions from a boat engine near the SIO pier. (a) 10 Hz timeseries of O₃, NO₂, and O_x (O₃ + NO₂) demonstrating ability to capture transient titration events. (b) Regression of O₃ and NO₂ plotted with a reference line of slope -1, showing conservation of total O_x at 10 Hz during a NO titration event.

1065

1070

Response to Reviewers

Comments for all Reviewers: We thank all reviewers for their time and thoughtful comments which have substantially improved the quality and clarity of our manuscript! Below we highlight three alterations to the manuscript, based on reviewer comments, which we believe are relevant for all reviewers. These changes have not necessitated changes to any of the conclusions of this work but have meaningfully improved the quality of our data treatment.

- 1) Based on very helpful comments from Reviewer 1, several portions of the eddy covariance data processing and quality control have been altered. In particular, we have devised a friction velocity filter based on agreement between our measured values and calculated values using the NOAA COARE v3.6 bulk flux algorithms, rather than a fixed friction velocity threshold. This has increased the number of valid quality controlled flux periods and improved our ensemble flux LOD. We have also applied a frequency attenuation correction to our flux values which resulted in a mean increase in $v_d(O_3)$ of 4.5%. These changes necessitated updating all reported EC flux values in the text and in Table 2, and Figures 6, 9, 12, S9, and S12. The updated mean campaign $v_d(O_3)$ is 0.013 (changed from 0.011 cm s^{-1} in the original manuscript) and the ensemble LOD is 0.0027 cm s^{-1} (changed from 0.0042 cm s^{-1}). The total number of valid quality-controlled flux observations is now 246 (changed from 151). Further details on each of these corrections are described in specific responses to Reviewer 1. We believe these changes, made directly following recommendations of the reviewer, have significantly enhanced the quality of our manuscript.
- 2) Also based on helpful comments from Reviewer 1 who noted that our determined response time of 0.9 s seemed longer than expected, we have revisited our determination of the instrument response throughout the campaign. It became apparent that infrequently the automated bi-exponential decay algorithm we applied over weighted the second exponential and gave poor fitting results. Instrument response times for O_3 have been recalculated using a single exponential decay fit which provides a better fit to the data. Calculated fits were manually verified for the full campaign. The updated response time is faster than the original reported value (0.28 s (0.25 to 0.31 s 95% confidence bounds), previously 0.9 s). Review of this response time calculation was also motivated by its direct use in the newly implemented frequency attenuation calculation described in comment number 1. This updated response time value was also used to calculate an updated value of the cutoff frequency (now 0.57 Hz, previously 0.18 Hz). This response time is more in keeping with expectations given that O_3 is a “non-sticky” gas and the high flow rates and low volumes in our instrument. The use of a single-exponential decay also follows the method of Bariteau et al. (2010) for the characterization of their fast-response chemiluminescence O_3 sensor. These values have been updated throughout the text. Additional discussion is provided in responses to Reviewer 1.
- 3) Based on private communications during the review process, we have included additional caveats in Section 5 regarding the conservation of total O_x observed during an O_3 titration from local NO emissions. In particular, it was noted that engine NO_x emissions cannot always be assumed to be exclusively as NO. Ship emissions have shown NO_x to NO_2

emission ratios on the order of 10%. If some emissions are indeed in the form of NO₂, the reported conservation of total O_x in section 5 would be partially spurious resulting from various compensating errors. We have added some discussion of this important point.

The manuscript has been revised to state in Section 4 : “This analysis assumes that there were no direct NO₂ emissions during the titration event. A NO₂ to NO_x emission ratio of 0.08 was observed for ship emissions from diesel motors on inland shipping vessels (Kurtenbach et al., 2016). Without additional knowledge amount the NO_x emission source during this event, the observed conservation of total O_x could be partially driven by compensating errors within 10%.”

Responses to individual reviewer comments follow. Reviewer comments are reproduced in italic black font. Author responses are shown in regular blue font. Text added to the manuscript is underlined and text removed from the manuscript has a strikethrough.

Response to Reviewer 1:

This paper describes the use of the oxygen anion chemical ionization mass spectrometer for simultaneous measurements of N₂O and O₃, with the application of eddy covariance flux measurements over the sea. It's another example of the versatile utility of the time-of-flight CIMS. The paper is generally well written and the authors have carefully considered the various aspects of data processing and interpretation. I recommend publication after they address the following mostly minor comments.

We are very grateful to the reviewer for their thorough review and numerous suggestions which have improved the quality of our data treatment and our manuscript as a whole. Below we address specific reviewer comments.

Abstract: Counts /s/ppt instead of ions/s/ppt

All instances of ions s⁻¹ pptv⁻¹ have been changed to counts s⁻¹ pptv⁻¹ or cps pptv⁻¹ (or ncps pptv⁻¹, etc.) as appropriate in the abstract and throughout the text to maintain consistency. We had used these terms interchangeably which was not made clear.

Line 53: authors introduced wet, dry, and gas-phase chemiluminescence methods here in this order, but discussed them subsequently in a different order (gas-phase, wet, dry). Suggest discussing the methods following the order of wet, dry, gas-phase

This point is well taken and the text has been rearranged as suggested but the content is unchanged.

Line 230. The increase in ncps of 175% doesn't quite square up with Fig. 5 by eye. This pressure sensitivity needs to be treated with care. How precise/accurate is the pressure in the IMR controlled? On a mobile platform (e.g. ship), motion sometimes can induce a pressure fluctuation. It would be good if the instrument can keep the pressure very accurate and constant, even in the presence of motion.

We thank the reviewer for catching this arithmetic error. The increase in absolute numbers was from 4.37E5 to 6.97E5 ncps. This corresponds to a 60% increase, or a signal at 95 mbar that is ~160% of the signal at 70 mbar. This value has been corrected and the text slightly clarified.

So far we have focused on ground based deployments at fixed sampling sites for the Ox-CIMS and so have not made significant efforts to ensure highly accurate pressures. The standard deviation of IMR pressure during individual flux sampling periods were typically from 0.1-0.3 mbar which would have a negligible impact on our observations. Methods for accurate and constant pressure control for CIMS instruments have been developed for airborne studies (i.e Lee et al. (2014)) and should be directly translatable to this instrument. This type of pressure control would be a useful addition before any airborne or ship-based deployments of the Ox-CIMS.

The manuscript has been revised to state: The normalized signal of O₃ increases by 175% 60% at an IMR pressure of 95 mbar compared to 70 mbar over the pressure range of 70 to 95 mbar in the IMR when sampling a constant O₃ source of 35 ppbv.

Line 245. Have the authors compared this N2 background vs. simply scrubbing the measured air (e.g. with activated charcoal)? The differences in H2O and CO2 between ambient air and scrubbed air are much smaller than those between ambient air and N2. This should make the background measurements easier to interpret.

The use of a scrubber will absolutely be explored before any future deployments. We also intend to explore the development of catalytic zero air generator to overflow the inlet which would maintain near ambient CO₂ and H₂O. In this initial deployment we had also aimed to measure a variety of other trace gases detectable with the O_x-CIMS not discussed in this manuscript. It was decided that the N₂ background was the most versatile method for zeroing all species of interest even if it necessitated additional considerations for O₃. Future deployments could implement a combination of scrubber-based zeros for O₃ and N₂ overflow zeros for other species to remove this issue.

Section 2.9. authors have shown that O3 normalized sensitivity is linear (up to 80 ppbv), despite the fact that CO3- signal and O2- signal being comparable in magnitude. They have also shown that NO2 normalized sensitivity doesn't depend on O3 level. Does the O3 normalized sensitivity depend on the NO2 concentration?

We have not directly assessed the dependence of O₃ normalized sensitivity on NO₂ but this will be a valuable future laboratory experiment, especially if we intend to sample in an urban high NO_x environment. We can note that the ambient normalized O₃ signal was insensitive to the high concentration formic acid standard additions described in this deployment which we expect to behave similarly to NO₂.

Paragraph beginning on line 317. This paragraph isn't very clear. How is it that above 1e6 cps, precision no longer improves with count rate, yet "For 10 Hz averaging and count rates of 1e6 and 1e7 cps, the corresponding instrument precision is 0.75 and 2% respectively, and appears independent of count rate"? Also, it would help the readers to spell out how the counting noise is computed.

We agree this section was confusing as written and have improved phrasing to clarify this discussion. The quoted sentence was primarily intended to show that from 1E6 to 1E7 cps instrument precision did not continue to improve with count rate. Instrument precision below 1E6 cps did improve with count rate as expected when precision is controlled by counting noise. The meaning of the observed precision at 1E6 and 1E7 cps being specifically 0.75 and 2% is not clear and is again only meant to highlight that precision is no longer improving with count rate as expected for counting noise. The equation for counting noise has been added which is $\frac{\sqrt{N}}{N}$ where N is the number of counts during the observation period.

The manuscript has been revised to state: "From this assessment, precision was observed to improve approximately linearly in a log-log scaling for count rates between 1×10^3 and 1×10^6 cps (Fig. S8) as expected in the case where counting noise drives instrument precision. Above 1

~~x 10⁶ cps there is an apparent asymptote where precision no longer improves with count rate. For 10 Hz averaging and count rates of 1 x 10⁶- and 1 x 10⁷-cps, the corresponding instrument precision is 0.75 and 2% respectively, and appears independent of count rate. The counting noise limited 10 Hz precision for 10⁶ and 10⁷ cps is are 0.32% and 0.1% respectively, while the measured values were 0.75 and 2%. The counting noise limited precision is calculated as \sqrt{N}/N where N is the number of counts during the integration time.”~~

Line 339. Without being familiar with these TOFMS or exploring the Vermeuel et al. reference, it's unclear how this O3 calibration factor is applied. You could refer readers to section 3.2.1 here.

and

Section 3.1 suggest adding 1-2 sentences describing how the CIMS was deployed. Was it subsampling from a inlet manifold like on Scripps pier? Length of inlet? Instrument temperatures?

Based on discussion from Reviewers 1 and 2, significant details have been added back to this section rather than requiring the reader to refer to Vermeuel et al. (2019).

The manuscript has been revised to state: Section 3.1: “The Ox-CIMS was located on the roof of a trailer (approx. 5 m above ground) and sampled through a 0.7 m long, 0.925 cm i.d., PFA inlet. The inlet was pumped at flow rate of 18-20 slpm from which the Ox-CIMS subsampled at 1.5 slpm. Temperature and RH were recorded inline downstream of the subsampling point. The Ox-CIMS sampling point was approximately 10 m horizontally from the Thermo-Fisher 49i and sampled at approximately equal heights. Instrument backgrounds of the Ox-CIMS were determined every 70 minutes by overflowing the inlet with dry UHP N₂. Calibration factors for O₃ were determined by sealing the in-field continuous addition of a C-13 isotopically labelled formic acid standard to the tip of the inlet. Laboratory calibrations of the Ox-CIMS to formic acid and O₃ as a function of specific humidity were determined immediately pre- and post-campaign and were used to calculate a humidity dependent sensitivity of O₃ relative to formic acid. That relative sensitivity was then used to determine the in-field sensitivity to O₃ by scaling field sensitivities of formic acid from the continuous additions. Full details of this deployment and calibration methods are described in Vermeuel et al., (2019).”

Line 342. The difference between the two instruments warrants further investigation. Even at 80 ppb the two instruments don't perfectly agree. Did the EPA monitor have a Nafion dryer to remove water vapor? What's the response time of the EPA monitor? If fairly slow, then during an O3 titration event due to NO the CIMS would initially see lower O3 than the EPA monitor at 1-minute resolution.

We agree that there remain open questions in this instrument comparison which are difficult to assess with the data available. While agreement between the two instruments is not perfect, we believe they show strong agreement for field sampling in a complex environment, especially as we are comparing to a monitoring grade instrument. The Thermo Fischer 49i (EPA O3 monitor) was not equipped with a Nafion drier and the manufacturer quoted response time for the instrument alone is 20 seconds. An additional unquantified response time of similar magnitude was likely present due to the instrument sampling from a long, wide diameter inlet at a low flow rate. Unfortunately, specific details of EPA O3 monitor inlet configuration were not recorded

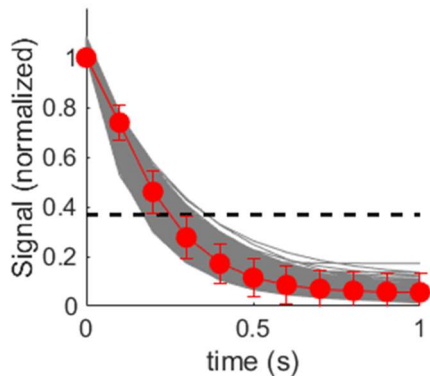
during this deployment, as it was not originally devised as an O₃ intercomparison study. Taken together, the EPA O₃ monitor was likely subject to interferences from water vapor and other species and had a slower response to titration events and changes in air masses. We also note that O₃ mixing ratios exceeding 80 ppbv were only sampled on three afternoons during the study, which were driven by highly polluted urban airmasses from Chicago, making robust comparison between the instruments at high mixing ratios a challenge. An instrument intercomparison study with a research grade O₃ instrument, such as an NO chemiluminescence sensor, rather than a monitoring grade instrument like the Thermo Fischer 49i will be valuable in further characterizing the Ox-CIMS.

Line 358. The authors have not discussed how their measurements might depend on the front block and IMR temperatures. Does temperature affect the stability of the clusters in the multi-step reactions? Also, does the use of 40 deg. nlet line have any affect on O3/heterogenous chemistry within the inlet?

The inlet temperature of 40°C was primarily selected to ensure that the inlet line was always held above ambient temperatures to prevent any potential condensation of water vapor in the line and to ensure consistent sampling conditions. Additional impacts on heterogeneous chemistry or ion-adduct stability were not quantitatively assessed. We speculate that these effects would be minor due to being only slightly above ambient temperatures (ca 25°C).

Line 392. These are pretty high flow rates. I'm not familiar with the internal volumes of the mass spec, but would've expected to see a faster response time than the 0.9 s quoted here. A couple of questions: 1. Are the authors confident that the N2 overflow tube consisted of N2 only (i.e. no diffusion of ambient air into that tube)? From experience, even when using a fairly thin tube (1/8" OD) to tee into the main manifold, there can be some diffusion of ambient air into the N2 line if it's just an open tee. This can be overcome by either having the shut-off valve next to the tee, or by doing the N2 puff multiple times in succession. 2. Alternatively, could the fairly low response time be due to the multi-stage chemistry?

Based on the reviewer's comments we have revisited our determination of the instrument response throughout the campaign. It became apparent that the automated bi-exponential decay algorithm we applied frequently over weighted the second exponential and gave poor fitting results. Instrument response times for O₃ have been recalculated using a single exponential decay fit which provides a better fit to the data. Calculated fits were manually verified for the full campaign. The updated response time is faster than the original reported value (0.28 s (0.25 to 0.31 s 95% confidence bounds), previously 0.9 s). Review of this response time calculation was also motivated by its direct use in the newly implemented frequency attenuation calculation described in comment number 1. This updated response time value was also used to calculate an updated value of the cutoff frequency (now 0.57 Hz, previously 0.18 Hz). This response time is more in keeping with expectations given that O₃ is a "non-sticky" gas and the high flow rates and low volumes in our instrument. The use of a single-exponential decay also follows the method of Bariteau et al. (2010) for the characterization of their fast-response chemiluminescence O₃ sensor. These values have been updated throughout the text. See below for a plot of single-exponential decays fits determined throughout the full campaign shown as grey traces, and the binned mean decay curve shown in the red trace. The dashed horizontal line is at 1/e which corresponds to the response time.



Eq. 4. Suggest replace KH with just H, to avoid confusion with Kt.
This terminology has been changed as suggested.

Line 427. This sentence very confusing. Suggest rewrite: “Outliers in $v_d(O_3)$ and the flux limit of detection were determined and removed for points three scaled median absolute deviations from the median. “

We appreciate this note and have updated the text as suggested.

Line 429. 84% flux rejection is clearly not ideal. Instead of applying a simple u^* threshold, I encourage the author to investigate the u^* and C_d vs. wind speed relationship. This stress relationship is fairly well known over the ocean, and the authors could choose to reject O_3 flux values when the measured u^* or C_d is far from expected.

We are grateful to the reviewer for this suggestion which we have implemented as follows. We have calculated the expected U^* for each flux period using the NOAA COARE v3.6 bulk flux algorithms, using observed wind speeds, SST, air temperature, and humidity as inputs. Flux periods were rejected if the calculated U^* was within 50% of the observed value. This filter resulted in a total of $N = 246$ valid flux points, mean $v_d(O_3) = 0.013 \text{ cm s}^{-1}$ and ensemble LOD of 0.0027 cm s^{-1} . We note that we are relatively insensitive to the specific threshold applied, selecting a threshold of 40% agreement yields $N=191$, $v_d(O_3) = 0.0137 \text{ cm s}^{-1}$, and $LOD = 0.0032 \text{ cm s}^{-1}$. A threshold of 30% agreement yields $N=138$, $v_d(O_3) = 0.0145 \text{ cm s}^{-1}$, and $LOD = 0.0027 \text{ cm s}^{-1}$. We have selected the threshold that minimizes the LOD while maintaining more valid flux points than the fixed U^* filter of 0.1 cm s^{-1} . We would also like to point out that the 84% flux rejection included the wind direction filter which may not have been clear. Over 30% of flux points were immediately rejected based on winds not coming from the ocean. We also note that even in the case of the 30% agreement threshold the ensemble LOD was improved compared to our original fixed U^* threshold. This suggests that this relative threshold does a better job of filtering low quality flux periods.

The text has been updated substantially in Section 3.3 to account for these changes.

Line 455. The lag time determined from maximum covariance is approximately half as much as those computed from the gas evacuation. I suppose this could be due to either a time error between the O₃ and wind measurement, or the fact that the inlet pressure is much lower than 1 atm (such as the volumetric flow rate is ~2x the mass flow rate).

The slight disagreement of these values was also notable to us. We believe the source of this is likely due to a timing error as suggested by the reviewer as the software saving the mass spectrometer and anemometer data signals were not optimized to have highly precise timing. The inlet pressure is also a likely contributing factor as suggested. A quick calculation of expected pressure drop in our inlet suggest that pressure at the Ox-CIMS subsampling point is ~150 mbar lower than ambient. As noted by the reviewer, this pressure drop will increase the volumetric at a given measured mass flow rate. Taken together we expect these factors to explain our observed lag time. We note that applying a fixed lag time corresponding to the volumetric residence time results in a calculated $v_d(O_3)$ of 0.012 cm s⁻¹ compared the our value of 0.013 cm s⁻¹ using the fixed lag time.

Line 467. One wouldn't expect the lag time to be the same as the response time. If $t_0 = 0$ represents the time when the N₂ was injected into the inlet, the O₃ signal should start to drop ~1 s later, and reach 1/e of the initial value ~1.9 s after t_0 .

We agree that the total instrument response time should be the sum of the volumetric clearing time of the inlet and the instrument response time. In our case the determined lag time for eddy covariance also appears to be influenced by software timing consideration as noted above. In our determination of the instrument response time, we treated t_0 as the point immediately before the signal responded to the N₂ overflow. This is done to separate out determinations of the inlet lag time and the instrument response time. This follows the method used by Bariteau et al (2010), which based on our determination on. Additionally, the position of the solenoid valve controlling the N₂ overflow was only recorded at 1Hz which makes it difficult to resolve the lag time based on the when the solenoid was flipped. This is also why we were no able to determine the instrument lag time using the “puff method” described in Bariteau et al. Calculating the response time based on when the signal begins to respond rather when the solenoid flipped removes that imprecision.

Also, as noted in the comment we made above we have since revisited our determination of the instrument response time, with a new mean value of 0.28 s based on a single-exponential decay fit.

Line 495. One way to deal with estimation of high frequency flux loss without directly using the noisy O₃ cospectra would be to take an unattenuated cospectra (could be Kaimal, or could be the less noisy measured heat cospectra), attenuated it with a filter function (e.g. Eq. 7 in Bariteau et al. 2010), and compute the ratio between unattenuated and attenuated cospectra. Finally you can apply this ratio to your measured O₃ flux to get the unattenuated flux. The flux loss at high frequencies is pretty obvious despite the very low wind speed. So this correction is worth characterizing well.

We thank the reviewer for the push to treat this attenuation correction properly. We have implemented a frequency correction following this suggestion. Briefly, we calculated the unattenuated Kaimal cospectra (assuming an unstable boundary layer) for each individual flux measurement period. We then applied the low pass filter function described by Bariteau et al. (2010) using a fixed response time of 0.28 s to determine the attenuated cospectra. The ratio of the attenuated to unattenuated cospectra was then taken and used as a correction factor. The net effect of this correction was an increase of $v_d(O_3)$ of 4% (increased from 0.0127 to 0.0132 cm s^{-1}). The manuscript has been changed in many locations to account for this change.

The manuscript has been revised significantly in Section 3.4 to reflect these changes.

Line 523. This is most likely true. See www.atmos-meas-tech.net/9/5509/2016/ for example.

We thank the reviewer for bringing this to our attention. We have added a short discussion and citation to the text.

The manuscript has been revised to state: Line 523: “This has been demonstrated in an EC study utilizing a closed path H₂O sensor for EC flux measurements (through an 18 m long, 0.635 cm i.d. inlet, pumped at 18 slpm, comparable to the inlet used in this study) which showed complete attenuation above 0.1 Hz and overall attenuation of ~80% of the H₂O (latent heat) flux (Yang et al., 2016). However, without a direct measure of water vapor fluctuations collocated with the Ox-CIMS this is difficult to assess directly definitively rule out in our measurement.”

Section 3.7.1 it might be worth mentioning that emission of NO from other sources (e.g. ships) could also bias the O₃ flux measurement. Though the authors’ despiking of the O₃ signal probably removed such short-term ship emission-related O₃ titrations.

We agree that this point should be stated explicitly. As stated by the reviewer we expect the combination of the despiking and stationarity criteria will do a suitable job of filtering out the very short and longer titration events respectively.

The manuscript has been revised to state: Section 3.7.1: “There is also potential for short term anthropogenic emissions of NO (such as from a boat engine passing by the sensor) to create a flux divergence term. We expect that the combination of signal despiking and the flux stationarity criteria described in Section 3.3 will minimize the impact of this potential divergence term. Despiking will remove most short term (<1 s) emission events and the stationarity criteria will filter out any period where longer term titration events cause large changes in the observed flux within a flux measurement period.”

Section 3.7.2 My understanding is that a vertical gradient in flux does occur within the MBL when there’s a large entrainment flux, but this mostly applies to the region ABOVE the ‘constant flux layer’ (i.e. more relevant for aircraft studies). The constant flux layer latter is usually taken to be roughly the lowest 10% of the MBL. Within the constant flux layer, we typically assume that there isn’t a vertical gradient in flux, and the measured flux = surface flux. I’m not aware of people making H₂O flux measurements from a ship/buoy needing to worry about the entrainment flux, for example. Some more discussion/references on this topic would be welcomed.

Our exploration of flux divergence was inspired by the aircraft observations of Lenschow et al., (1982) which showed a linear flux divergence with altitude for measurements at 15, 60, and 325 m over the ocean. The boundary layer height during those flights was *ca* 1.2 km. The flux observations at the 15 and 60 m measurement heights showed strong divergence despite being in within the constant flux layer (based on the lowest 10% rule). Lenschow et al. (1982), argue that because the surface flux of O₃ is much smaller than the entrainment flux ($w_e = 0.8 \text{ cm s}^{-1}$), it is acutely sensitive to boundary layer processes. Faloon et al., (2005) also showed a linear flux divergence in O₃ down to 100m with a boundary layer height of ~800 m. There it is unclear if the lowest level leg was within the constant flux layer but still suggests that entrainment driven flux divergence should be considered. We realize that not citing and discussing Lenschow et al. (1982) in this section was an oversight and have revised the text to include discussion of their observations.

We also made our calculations directly following the equations in Blomquist et al. (2010) who assessed impacts of entrainment on near surface ($z_i = 18 \text{ m}$) observations of DMS flux. Blomquist et al. (2010) applied a linear extrapolation from the boundary layer height to the surface and did not invoke a constant flux layer. Based on these results we believe there is value in exploring this potential source of bias in our observations even if we do not have direct constraints on its magnitude.

The manuscript has been revised to add: “Lenschow et al., (1982) presented aircraft observations of O₃ deposition over the Gulf of Mexico at heights of 15, 60, and 325 m which showed a strong flux gradient term driven by entrainment from the free troposphere. The boundary layer height (z_i) during those flights was approximately 1.2 km, suggests a strong flux gradient was present even within the surface layer (approximated as the lowest 10% of the boundary layer).”

We also note the correction of a typo on line 571. z_i is the boundary layer height and z is the measurement height. These definitions were reversed in the text but were used correctly in Eq. 9 and all calculations following it.

Line 589. ‘Within range’ instead of ‘in good agreement’, since there’s a lot of variability in previous measurements.

This point is well taken, and the text has been updated using the reviewer’s phrasing

References:

Bariteau, L., Helmig, D., Fairall, C. W., Hare, J. E., Hueber, J. and Lang, E. K.: Determination of oceanic ozone deposition by ship-borne eddy covariance flux measurements, *Atmos. Meas. Tech.*, 3(2), 441–455, doi:10.5194/amt-3-441-2010, 2010.

Blomquist, B. W., Huebert, B. J., Fairall, C. W. and Faloon, I. C.: Determining the sea-air flux of dimethylsulfide by eddy correlation using mass spectrometry, *Atmos. Meas. Tech.*, 3(1), 1–20, doi:10.5194/amt-3-1-2010, 2010.

Faloona, I., Lenschow, D. H., Campos, T., Stevens, B., van Zanten, M., Blomquist, B., Thornton, D., Bandy, A. and Gerber, H.: Observations of Entrainment in Eastern Pacific Marine Stratocumulus Using Three Conserved Scalars, *J. Atmos. Sci.*, 62(9), 3268–3285, doi:10.1175/JAS3541.1, 2005.

Lee, B. H., Lopez-Hilfiker, F. D., Mohr, C., Kurtén, T., Worsnop, D. R. and Thornton, J. A.: An iodide-adduct high-resolution time-of-flight chemical-ionization mass spectrometer: Application to atmospheric inorganic and organic compounds, *Environ. Sci. Technol.*, 48(11), 6309–6317, doi:10.1021/es500362a, 2014.

Lenschow, D. H., Pearson, R. and Stankov, B. B.: Estimating the ozone budget in the boundary layer by use of aircraft measurements of ozone eddy flux and mean concentration, *J. Geophys. Res.*, 86(C8), 7291, doi:10.1029/JC086iC08p07291, 1981.

Responses to Reviewer 2:

This paper describes the development and application of an oxygen anion chemical ionization mass spectrometry approach for directly measuring the flux of ozone and nitrogen dioxide. Of particular note, is the successful application of this technique in the marine boundary layer where the magnitude of O₃ and NO₂ fluxes is low. The authors describe thoughtful and extensive laboratory characterization, comparison with traditional measurements in the field, initial deployment for flux measurements, and data analysis and correction. The paper is well organized and clearly written. The comments and suggestions below are meant to improve an already very good paper.

We thank the reviewer for their supportive and thoughtful comments! Replies to all specific reviewer comments are below.

Specific Comments:

L35-39: Is there any experimental evidence that $v_d(O_3)$ depends on factors beyond wind speed and SST? e.g., surface ocean composition? Could such factors contribute to the order of magnitude range noted in L35? Do any measurements exist over snow ice? Or freshwater versus seawater?

Ocean surface composition is known to be a controlling factor in $v_d(O_3)$, with Iodide and various dissolved organic compounds (DOCs) being the primary contributors. Parameterizations to SST are primarily made as a proxy for iodide which is globally directly correlated with SST. In nearly all field measurements of $v_d(O_3)$, DOC and iodide were not measured. Instead laboratory studies of O₃ deposition to water containing DOC and iodide are used to model their role in ambient O₃ deposition. To our knowledge there is one EC measurement of O₃ deposition to freshwater (Wesely et al. (1980)) who reported a $v_d(O_3)$ of 0.01 cm s⁻¹. Incidentally we have a manuscript in progress applying the Ox-CIMS reported here for deposition measurements to lake water. Observations to snow vary widely but current best estimates suggest that deposition is slow (0-0.01 cm s⁻¹). Mention of these values has been added to the text. We have also added some discussion to the role of iodide and DOC in controlling O₃ to the text here.

The manuscript has been revised to state: Starting at Line 35: “There is only one reported study of O₃ deposition to freshwater, which showed $v_d(O_3)$ of 0.01 cm s⁻¹ (Wesely et al., 1981). Measured deposition rates to snow and ice vary widely, with most observations of $v_d(O_3)$ from 0 to 0.2 cm s⁻¹, while models suggest $v_d(O_3)$ from 0 to 0.01 cm s⁻¹ (Helmig et al., 2007). Reactions of O₃ with iodide and dissolved organic compounds (DOC) in the ocean are known to play a controlling role in setting $v_d(O_3)$ and may explain some of the variability in observations (Chang et al., 2004; Ganzeveld et al., 2009). However, these quantities have not typically been measured during field studies of $v_d(O_3)$.”

L53: Is it worth pointing out explicitly here, for the non-expert reader, that UV photometric detection of O₃ doesn't provide fast enough time response for flux measurements?

We agree this is important to state explicitly and have added this discussion as suggested.

The manuscript has been revised to state: Starting at Line 53: “Due to this constraint, standard O₃ monitoring instruments which utilize UV-absorption detection do not have suitable time response or precision for EC measurements and ozone flux measurements have primarily utilized fast response chemiluminescence sensors.”

L110-111: Which type of ToF is used here? e.g., HToF or CToF?

We use a CToF with resolution of *ca.* 950 at the CO₃- product (-m/Q 60). We have updated the text to state this more explicitly.

The manuscript has been revised to state: Line 110: “the ion beam for entry into the compact ToF mass analyzer (CToF,...)”

L126-127: Any reference for “a wide class of molecules”? Or, can the authors be slightly more specific? e.g., hydrocarbons/oxygenates/S-containing/N-containing etc

The text as written was likely too vague and we have removed the phrase “a wide class of molecules” and instead point the reader to a review paper which compiled electron affinity measurements and calculations. This reference provides the reader with a starting place to easily assess if the Ox-CIMS has potential to measure a molecule of interest.

The manuscript has been revised to state: Line 126: “...resulting in a relatively non-specific reagent ion chemistry ~~which is sensitive to a wide class of molecules~~ (see Rienstra-Kiracofe et al., (2002) for a compilation of molecular E.A. values.)”

L181-189 (and elsewhere): Is ions/s used equivalently with counts/s? Does one quantity rely on the calibration of the single ion signal? A clear definition would be helpful.

Thank you for pointing out this ambiguity. Ions s⁻¹ and counts s⁻¹ are equivalent and were used interchangeably throughout the text. We have changed all instances of ion s⁻¹ or related expressions throughout the text to counts s⁻¹ (or cps/ncps as appropriate) for clarity.

L187: Does this mean that signals are normalized to a fixed value? Or normalized to the variable signal for a reagent ion? Or, does this refer to the signal/pptv you would obtain for a reagent ion signal of 1e6 ions/s? Clarification would be helpful.

We normalize signals by scaling to a fixed total reagent ion signal of 1E6 cps. This follows the standard approach in many CIMS applications. Based on suggestions from Reviewers 2 and 3, this section has been clarified.

The manuscript has been revised to state: Line 187: “Sensitivity values can be normalized by scaling all signals to a fixed total reagent ion signal count rate of 1 × 10⁶ cps ions s⁻¹ to isolate the sensitivity component controlled by reagent ion chemistry, separate from total instrument count rate changes in instrument performance due to decay in the ion source or other factors. The total reagent ion signal is taken as the sum of the O₂⁻ and O₂(H₂O)⁻ signals.”

L223-224: Reference or supplemental data for this statement?

This statement as written was likely an overstatement based on the amount of evidence we currently have. Laboratory calibrations of formic acid, H₂O₂, NO₂, and nitric acid have shown insignificant difference when performed in N₂ or in ambient air. Beyond that we have not performed a robust set of experiments to specifically rule out the involvement of CO₂ in the detection of other analytes. We have revised the text to be less definitive and acknowledge that only a small set of molecules have been specifically calibrated.

The manuscript has been revised to state: Line 223: “No other analytes that we have calibrated for analyzed with the Ox-CIMS (HCOOH, HNO₃, H₂O₂) have shown a CO₂ mixing ratio dependence, demonstrating suggesting that CO₂ may be is uniquely involved in the detection of O₃ this mechanism and is not a general feature of the oxygen-anion chemistry.”

L292-293: Are signals only normalized to the reagent ion when the reagent ion is lower than the analyte signal?

Ambient data was normalized for all analyte signal magnitudes. This is necessary for applying laboratory humidity dependent sensitivities to ambient observations despite slow drift in instrument performance.

L331 (section 3.1): The next section (3.2) contains quite a lot of detail on instrument set up in the field (temperatures, inlet etc.), but relatively little information is given here. More detail would be useful.

And

L339-341: Somewhat more detail on this scaling and how it is assessed/applied is warranted here, rather than relying heavily on the Vermeuel reference.

Based on discussion from Reviewers 1 and 2, significant details have been added back to this section rather than requiring the reader to refer to Vermeuel et al. (2019).

The manuscript has been revised to state: Section 3.1: “The Ox-CIMS was located on the roof of a trailer (approx. 5 m above ground) and sampled through a 0.7 m long, 0.925 cm i.d., PFA inlet. The inlet was pumped at flow rate of 18-20 slpm from which the Ox-CIMS subsampled at 1.5 slpm. Temperature and RH were recorded inline downstream of the subsampling point. The Ox-CIMS sampling point was approximately 10 m horizontally from the Thermo-Fisher 49i and sampled at approximately equal heights. Instrument backgrounds of the Ox-CIMS were determined every 70 minutes by overflowing the inlet with dry UHP N₂. Calibration factors for O₃ were determined by sealing the in-field continuous addition of a C-13 isotopically labelled formic acid standard to the tip of the inlet. Laboratory calibrations of the Ox-CIMS to formic acid and O₃ as a function of specific humidity were determined immediately pre- and post-campaign and were used to calculate a humidity dependent sensitivity of O₃ relative to formic acid. That relative sensitivity was then used to determine the in-field sensitivity to O₃ by scaling field sensitivities of formic acid from the continuous additions. Full details of this deployment and calibration methods are described in Vermeuel et al., (2019).”

L356-358: How do these temperatures impact instrument performance? Is it species dependent?

The primary motivation for these temperatures was to ensure that the inlet and instrument front end temperatures were always higher than ambient temperatures to prevent any condensation of water vapor. O₃ is typically considered a “non-sticky” molecule and is likely not significantly impacted by the selected temperature as long as it is ensured that there is no condensation of water.

L429: Does 84

It appears the Reviewers comment here was lost somewhere in the uploading process but we will provide additional detail here to hopefully answer their question. The 84% rejected flux periods refers to all ambient sampling periods, including those where winds were not from the ocean. The wind direction filter removed approximately 30% of the campaign data, followed by an additional 57% reduction due to the u* filter and further cuts due to the stationarity and outlier filters.

Additionally, please note that all values in this section have been revised as described in Comment 1 to all reviewers.

L431: How does ‘despiking’ impact the results?

The despiking algorithm as applied is intended to remove short large spikes in the data, primarily driven by electronics issues. If these short electronic spikes were left in the data they could bias the observed flux value and increase the LOD, as they would drive a strong short covariance signal. This despiking correction and our specific implementation are standard in EC data processing. Such spikes were negligible in our dataset and the correction was applied for completeness.

L520-521: For the non-expert reader it may be useful to clarify whether this bias is specific to O₃ measurement with Ox-CIMS, or to CIMS measurements of trace gases in general.

We agree that this is a useful point to clarify. This correction would impact all CIMS instruments as they also measure mixing ratios relative to moist air with variable density. Due to the high mixing ratios of O₃ and the small deposition magnitude to water, measurements of O₃ air-sea exchange are particularly sensitive to this potential bias. Still, this factor should be considered for all flux sensors that do not directly measure mole fractions or mixing ratios relative to dry air.

The manuscript has been revised to state: Line 520: “The Ox-CIMS measures O₃ as the apparent mixing ratio relative to moist air, as is true of all CIMS based measurements, which means fluctuations in the density of air due to changes in temperature, pressure, and humidity could introduce a bias in the EC flux measurement (Webb et al., 1980).”

L766-767: incomplete citation to Vermeuel 2019. doi?
Thank you, this citation has been corrected.

Technical Corrections:

L194: “was seen to have” to “had”

L223: “analytes analyzed” to “analytes detected/measured”

L305: Repeated section title? (Same as 2.9)

L527: Repeated phrase “which is removed by active heating of the inlet”

L528: semicolon use

L590: validation to validate

We thank the reviewer for their careful reading! All of the above technical corrections have been made following the suggestions of the reviewer.

The title of Section 2.10 was indeed accidentally copied from the title of Section 2.9. The title of Section 2.10 has been corrected to: “Short- and long- term precision”

Responses to Reviewer 3:

General comments:

A novel method of measuring O₃ and NO₂ based on chemical ionization time-of-flight mass spectrometry with oxygen anion (O₂⁻) as the reagent ion (Ox-CIMS) is developed. This new method is able to measure O₃ and NO₂ at fast time response and low mixing ratios, which is applicable to eddy covariance flux measurements. The authors conducted thorough characterization of the sensitivity, ion chemistry, inlet, calibration in the laboratory. They also used the instrument for the measurement of O₃ vertical fluxes over the coastal ocean, via eddy covariance. Their measured flux is in good agreement with prior studies of O₃ ocean-atmosphere exchange. Potentially, fluxes for multiple species can be obtained with one measurement with the Ox-CIMS. During the same campaign, they also used a 2B ozone monitor to measure ozone, which agreed well with the Ox-CIMS measurement. The paper is well written, and I suggest publishing this work after addressing the following specific comments.

We thank the reviewer for their thoughtful and supportive review. Responses to specific reviewer comments are below.

Specific comments:

- 1.) Around line 138 to 153 on the discussion of CO₃⁻ ion formation, do other chemicals also form CO₃⁻? It was mentioned early on line 119 that SO₂ also forms CO₃⁻? How to rule out that CO₃⁻ detected are not from other chemicals? Similarly, on line 215, would CO₃⁻ come from other species, rather than O₃+CO₂+O₂-chemistry?

We believe the discussion of use of CO₃⁻ reagent ions for detection of SO₂ was confusingly worded. In that work, SO₂ does not generate CO₃⁻, rather CO₃⁻ reagents are used to ionize SO₂ forming SO₃⁻. We highlighted this prior work as CO₃⁻ reagent ions were made by first generating O₂⁻ ions and reacting them with intentionally added O₃ in the presence of CO₂. In our work the same mechanism is used, but rather than intentionally adding excess O₃ to form CO₃⁻, we detect ambient O₃ in the form of the CO₃⁻ product.

We believe it is unlikely that other species significantly compete with the O₃+CO₂+O₂-chemistry. For a species to favorably transfer an O⁻ to CO₂ it must be a strong gas phase oxidizing agent and form a more stable product following O⁻ transfer. It is apparent what species might follow the above requirements. Those species if present are also likely highly reactive oxidized molecules which would be at low mixing ratios relative to O₃.

The manuscript has been revised to state: starting at line 118 “Oxygen anion chemistry has also been used for the detection of SO₂ via a multi-step ionization process where CO₃⁻ reagent ions are first generated by the reaction of O₂⁻ with added excess O₃ in the presence of CO₂. The CO₃⁻ reagent ion product then ligand switches with SO₂ to form SO₃⁻ which then quickly reacts with ambient O₂ to form the primary detected SO₅⁻ product (Porter et al., 2018; Thornton et al., 2002a).”

- 2.) *Line 154: Are there other interfering species that will end up as NO₂⁻ in the CIMS? Do HNO₃, HONO, PAN or Organ-NO₂ form NO₂⁻ with the ion chemistry? For example, on line 282, the authors mention that “A possible source of this background is from degradation of other species such as nitric acid or alkyl nitrates on the inlet walls.” Did the authors do any test for interfering species?*

We agree that this is an important consideration that should be made clear to the reader. We have not yet extensively tested for other potential interfering species at the NO₂⁻ product. Laboratory and field calibrations of HNO₃ do not show contribution to the NO₂⁻ product, but a small fraction is seen as NO₃⁻. The conservation of total odd-oxygen during an O₃ titration event discussed in Section 4 gives some qualitative indication that interfering species are likely small, but more direct evidence is necessary. Further validation of the NO₂ detection product is certainly warranted to characterize any interferences but we believe that to be beyond the scope of this work. The manuscript focuses primarily on the O₃ measurement and we tried to be upfront that the NO₂ measurement currently has less validation than the O₃ measurement. We make further reference to this in section 5 (Conclusions and outlook) stating “Further optimization and characterization of the Ox-CIMS is ongoing, including efforts to validate the specificity of the NO₂ detection...”

The manuscript has been revised to state: Line 282: “Additional calibration will be necessary to ensure that observed NO₂ signal is not a secondary product of other species and we cannot currently quantify their potential interference on measured NO₂.”

- 3.) *Line 189, can the authors specify what the normalized counts are? Is it normalized to the reagent ion counts?*

Based on suggestions from Reviewers 2 and 3, discussion of the normalization of the normalization process has been clarified. Generally, we use it in the same way as is common in chemical ionization mass spectrometry applications, where all signals are scaled relative to a fixed total reagent ion signal of 1×10^6 cps.

The manuscript has been revised to state: Line 188: “Sensitivity values can be normalized by scaling all signals to a fixed total reagent ion signal of 1×10^6 cps to isolate the sensitivity component controlled by reagent ion chemistry, separate from ~~total instrument count rate changes in instrument performance due to decay in the ion source or other factors.~~ The total reagent ion signal is taken as the sum of the O₂⁻ and O₂(H₂O)⁻ signals.”

- 4.) *Section 2.8: The authors mentioned that background measurement influences the detection limit. Do they have any recommendation in improving the detection limit?*

Because the instrument O₃ background is driven by chemistry in the reagent-ion source it is not clear what best approach is for reducing this background. We speculate that use of an alternative ionization source (*i.e.* soft x-rays or a corona discharge) may reduce this background issue but that would require laboratory work beyond the scope of this work. Alternatively a mass selective filter at the interface of the ion source and the IMR could be

used to remove the larger O_3^- ions (-m/Q 48) and preserve the O_2^- reagent ions (-m/Q 32) which would also be a substantial undertaking.

5.) *Line 572: It might be easier for readers to include the equation in the paper and cite Bariteau et al., so readers won't need to download Bariteau et al.*

The equations from Bariteau. 2010 have been added to the text as suggested. In the course of revising the text, we realized a citation of Lenschow and Kristensen (1985) was also warranted, which has also been added.

The manuscript has been revised in this section to list the equations and define all variables starting at Line 572.

References:

Lenschow, D. H. and Kristensen, L.: Uncorrelated Noise in Turbulence Measurements, J. Atmos. Ocean. Technol., 2, 68–81, doi:[https://doi.org/10.1175/1520-0426\(1985\)002<0068:UNITM>2.0.CO;2](https://doi.org/10.1175/1520-0426(1985)002<0068:UNITM>2.0.CO;2), 1985.